

Vibration and Audio Measurements in the Monitoring of Basic Oxygen Furnace Steelmaking



JUHANI NISSLÄ, MIKA PYLVÄNÄINEN, VILLE-VALTTERI VISURI,
PASI RUOTSALAINEN, JOUNI LAURILA, ATTE RANKINEN,
TUOMAS PALOVAARA, and TONI LIEDES

A basic oxygen furnace (BOF) is the main unit process for refining carbon steel. The aim of this work was to study the use of vibration and audio signal measurements to monitor, predict, and control the BOF process. Vibration and audio data from nearly 300 blows were collected and analyzed together with process variables. We could confirm high correlations between some of the process variables and vibration and audio measurements. Median filtered low-frequency (3–20 Hz) audio as well as X- and Z-direction acceleration root mean square (RMS) time series correlate with the off-gas temperature, although this is much more significant for the audio data. For Y-direction measurements (the upward direction) the correlation is negligible. The low-frequency audio and vibration data are likely related to the rate of decarburization. Median filtered mid-frequency (100–1000 Hz) audio as well as X-, Y-, and Z-direction acceleration RMS time series correlate with the lance height measurement during the interval 20–600 seconds from the beginning of oxygen blow. For the audio data, the correlation was high even without median filtering. We suggest that audio and vibration activity in this frequency range is possibly related to the formation of the metal–slag–gas foam and maybe even to slopping.

<https://doi.org/10.1007/s11663-023-02859-5>
© The Author(s) 2023

I. INTRODUCTION

THE overall purpose of the BOF process is to reduce the carbon content from about 4–4.5 wt pct to less than 1 wt pct (usually less than 0.1 wt pct), to reduce or control the sulfur and phosphorus contents, and to raise the temperature of the liquid steel made from scrap and hot metal to approximately 1600 °C–1700 °C. The oxidation of carbon to CO and CO₂ is the most extensive and important reaction in this process and it is achieved by injecting high-purity oxygen at supersonic velocities using a water-cooled top lance fitted with a convergent-divergent lance head. Main stirring is caused

by carbon burning and additional stirring of the metal bath is provided with gas injection through porous plugs in the bottom of the furnace.^[1] The chemical reactions and dynamics of the BOF process are described in more detail in References 2 and 3.

High-speed films from crucible tests with hot metal have shown that the depth and diameter of the depression produced by single and multi-nozzle jet oscillate both in vertical and horizontal directions roughly at the frequency of 10 to 12 Hz.^[4] In Reference 5 an accelerometer mounted on top of an oxygen lance was used to estimate the amount of slag formation during the BOF process. The technique utilized the vibration level as a basis to adjust the lance height and thus control slag formation.

Brämning et al.^[6] have studied the use of vibration measurements for foam level detection during the oxygen blows and in Reference 7 also audio measurements from above the converter were utilized. In those studies, the emphasis was on vibration frequencies below 20 Hz and sound frequencies below 1000 Hz. Sound measurements were also utilized in Reference 8 to detect the three different cavity modes formed into the surface of the liquid by the oxygen blowing (*i.e.*, dimpling, splashing, and penetrating), although only a cold air–water model was used in the experiments of that study. De Vos *et al.*^[9] have compared different foaming indices and found them not so effective in the industrial environment. They also mention in Reference

JUHANI NISSLÄ, MIKA PYLVÄNÄINEN, JOUNI LAURILA, ATTE RANKINEN, and TONI LIEDES are with the Intelligent Machines and Systems, University of Oulu, PO Box 4200, 90014 Oulu, Finland. Contact e-mail: juhani.nissila@oulu.fi VILLE-VALTTERI VISURI is with the Process Metallurgy Research Unit, University of Oulu, PO Box 4300, 90014 Oulu, Finland. PASI RUOTSALAINEN is with the Applied and Computational Mathematics, University of Oulu, PO Box 4500, 90014 Oulu, Finland. TUOMAS PALOVAARA is with the Technical Development, Steelmaking, SSAB Europe Oy, PO Box 93, 92101 Raahe, Finland

Manuscript submitted January 31, 2023; accepted June 30, 2023.
Article published online September 1, 2023.

9 that slopping typically occurs when 30–40 pct of oxygen is supplied. Birk *et al.*^[10] estimated foam height in a water model using sound measurements and they also compared the results to a measurement from a LD converter. In the test setup, a sound frequency range of 2–11 kHz was attenuated by the foam, but for the actual converter measurement they provide a spectrum from the lower range of 100–500 Hz and imply that this region is attenuated by increasing foam height.

The use of sound measurements for predicting the endpoint of the metallurgical reactions was discussed already in the 1970s^[11] and 1980s.^[12] In the documented discussion following the presentation of the study by Claes and Dauby^[12] Don McFarlane from the audience asked whether the sonic meter is used for both lance height and flow control. Jacques Claes answered that they had made a lot of experiments to measure foam height in high-frequency ranges and that in lower frequency ranges the microphone can be used to indicate the end of blowing in bottom blowing processes and that Figure 1 of their paper shows such a signal. The fact that measured signals from the BOF process contain different information in different frequency ranges is studied extensively in this paper, and thus we consider the mentioned discussion from almost 40 years ago as interesting and important. Nilles and Dauby^[11] also show a very early example of measured vibration intensity data from the BOF process in their Figure 14. The authors of Reference 11 noted that the recording of the vibrations with accelerometers might be relevant for the aspects of estimating the endpoint of the process. Another study of the vibration behavior in the BOF process^[13] modeled the cyclic formation and growth of CO bubbles due to the decarburization. The authors of the study^[13] then argued that this is the main cause of the vibrations. In Reference 13, it was shown that the CO content of the off-gas and the vibration intensity from one 350 t BOF heat seem to correlate a lot and both graphs seem to correlate with the expected carbon oxidation rate.

Mucciardi *et al.*^[14–16] have studied vibrations collected from the side of a laboratory scale BOF vessel, which could fit approximately 16 kg of hot metal. In References 14 and 15, some example heats are shown and the plots of cumulative vibrations (*i.e.*, integrated absolute values of the accelerometer signals) and their

average slopes. It seems that the slope of the cumulative vibration signal correlates with the typical decarburization rate curve of a BOF heat. In Reference 16 time series of accelerometer signal variance from five full test blows are shown. The authors in Reference 16 suspect that an accelerometer is sensitive not only to the gas formation in the decarburization process, but also to the operating parameters of the blow and especially the oxygen flow rate and lance height.

The measurements and findings of the cited previous studies are summarized in Table I. It is apparent that it is possible to get useful information from the BOF process by combining vibration and audio measurement data with other static and dynamic process measurements. Particularly interesting are the efficiency of carbon and phosphorus removal and the functionality of the bottom stirring. In fact, these factors cannot be measured (directly) at all during the process. In the recent review paper^[17] on slag foam height monitoring it was found that cold model results are difficult to relate with industry data and in real industrial settings there is still a fundamental lack of knowledge on acoustic behavior in dynamic liquid foaming.

The aims of this study were as follows:

1. Measure and compare vibrations from the trunnion pin of the vessel and from the fixed body. The goal of these pre-measurements is to see how much vibration information related to the BOF process is lost if it is measured from the fixed side.
2. Design a measurement system capable of measuring mechanical vibration from the vessel trunnion in X-, Y-, and Z-directions. The system operates autonomously on battery power and stores the signals in its own hard drive. The batteries and hard drives are changed at most once a day. A separate system is used for recording audio data from above the converter.
3. Implement a comprehensive measurement campaign for collecting data from the BOF processes for thorough analysis. The spectral content of the vibration and audio signals are analyzed and their correlations with some process parameters (lance height and off-gas temperature) are studied.

II. MATERIALS AND METHODS

All the measurements were conducted at SSAB Europe Raahe steelworks on a single 125-ton converter during its normal operation. The BOF has an ultrasonic lance with five nozzles and its bottom stirring is supplied through eight multi-hole plug (MHP) nozzles. Average oxygen flow rate is 350 m³/min and inert gas flow rate is 4000 L/min. Typical scrap-to-hot metal ratio is 18.4 pct.

A. Pre-measurements

Pre-measurements were carried out to determine the optimal measurement points to measure the vibrations of the BOF. Based on these measurements, it was found that distinctly more information is obtained about the

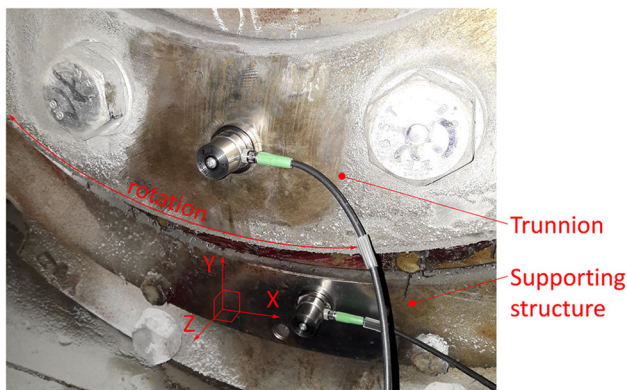


Fig. 1—The pre-measurement accelerometers in place when the converter is in its vertical, *i.e.*, operation position.

Table I. A Survey of Studies About Vibration and Sound Measurements of the BOF Process

Study	Year	Type of Vessel	Measurements	Findings
Nilles and Dauby ^[11]	1976	35-ton OBM/Q-BOP converter	audio and vibration measurements	the measurements analyzed together with gas composition, flame intensity, and slag and liquid compositions
Iida <i>et al.</i> ^[5]	1980	top blown converter, size of vessel not given	accelerometer on top of a lance, measured up to 600 Hz	sufficient slag formation and slopping monitoring possible via measurement of lance movement
Claes and Dauby ^[12]	1981	150-ton converters	microphone	endpoint of decarburization using sound intensity measurements
Mucciardi <i>et al.</i> ^[14,15]	1984, 1985	laboratory scale 16 kg hot metal tests	accelerometer	cumulative vibration amplitudes and their rate of change might correlate with decarburization rate, accelerometer data are sensitive to many parameters
O'Leary <i>et al.</i> ^[16]	1986	laboratory scale 15 kg hot metal tests	accelerometer on the side of the furnace, a photocell directed at the furnace and a cooling water thermocouple at exit of the oxygen lance	several unique time series of complete tests shown, including five accelerometer data variance curves
Koria and Lange ^[4]	1987	100 mm x 60 mm or 95 mm x 120 mm quartz crucibles	16 mm high-speed film camera	depth and diameter of depression mainly influenced by oxygen pressure, lance distance, and number of nozzles
Velichko <i>et al.</i> ^[13]	1997	350-ton top blown converter, smaller ones also mentioned	vibration sensor, type, and frequency range not specified	theoretical argument that cyclic formation and growth of CO bubbles due to the decarburization causes vibration of the vessel, CO content graph seems to correlate with vibration intensity
Birk <i>et al.</i> ^[10]	2001	water model and a converter	audio measurements, 2–11 kHz for the water model and 100–500 Hz for the converter	foam height dampens the frequency ranges mentioned, though only a single spectrum is analyzed for the converter
Brämning <i>et al.</i> ^[6,7]	2011	top blown converters with bottom mixing, 130-ton, and 300-ton sizes	accelerometer mounted on the trunion and a microphone above the converter, vibration frequencies analyzed up to 23 Hz and audio up to 1 kHz	time evolution of high-frequency audio and low-frequency vibration RMS values are studied and argued to correlate with dynamic foam height and slopping, but no convincing correlations are shown
Sabah and Brooks ^[8]	2016	cold air–water model and also motor oil to simulate slag	microphone, frequencies analyzed up to 7500 Hz	analysis of high-frequency sound measurements to study the three different cavity modes and the effect of second layer
De Vos <i>et al.</i> ^[9]	2021	330-ton top blown converter	audio measurements (frequency range not specified) and end of blow slag measurements	low acoustic measurements correspond to high foam heights, the calculated foaming indices are dominated by the slag's viscosity

vibration behavior of the BOF when the sensor is mounted to the trunnion pin of the vessel compared to the measurements of the fixed body.

The pre-measurement accelerometers were two MMF KS813B triaxial accelerometers attached at the bottom part of the rotating trunnion and its supporting structure as shown in Figure 1. Their nominal sensitivity is 100 mV/g in all directions and the linear (± 3 dB) frequency range is from 0.2 Hz to 10 kHz (Z-axis). X- and Y-direction are horizontal and vertical and perpendicular to the trunnion pin of the vessel. Z-direction is horizontal and parallel to the trunnion pin. The accelerometers were attached with magnets.

Since the vibration is generated inside the converter by the oxygen blowing and stirring of liquid metal with inert gases, it is valid to think that this vibration is further transmitted from the converter through the bearing of the rotating trunnion into its supporting structure. Thus, our hypothesis was that the bearing and the supporting structure act as a mechanical filter and the vibration is dampened when it passes through them. This mechanical filter can be modeled as a linear system. The vibration measured at the bottom part of the rotating trunnion is the input $x(t)$ to the system and the vibration measured at the supporting structure is the output $y(t)$. Taking Fourier transforms, we get from the theory of LTI systems that the frequency response of the mechanical filter is

$$H(f) = \frac{Y(f)}{X(f)}. \quad [1]$$

In practice, a more stable estimate is to assume that the measurements are random signals. Then the frequency response is calculated using the power spectral density S_{XX} and cross-spectral density S_{XY} . If we assume that the input \mathbf{X} is a weakly stationary random signal, then so is the output \mathbf{Y} and the frequency response of the LTI system can be characterized via the equation^[18]

$$H(f) = \frac{S_{XY}(f)}{S_{XX}(f)}. \quad [2]$$

We can also define the magnitude squared coherence between the random signals \mathbf{X} and \mathbf{Y}

$$\gamma_{XY}^2(f) = \frac{|S_{XY}(f)|^2}{S_{XX}(f)S_{YY}(f)}, \quad [3]$$

which measures the linear correlation between \mathbf{X} and \mathbf{Y} at the frequency f . For an ideal LTI system, the coherence is 1 at every frequency.

The estimated transfer functions and coherences were calculated from the middle part of a blow from short signal segments. They are shown in Figure 2 and the signal segments are shown in Figure 3. The transfer functions are very similar from all directions, and they all show that considerable amount of attenuation occurs. The coherences are not close to one at any frequencies and at higher than 7 kHz they are mostly less than 0.01. This means that either the simple linear model of vibration transfer is incorrect, or that there are

other inputs to our measurements or noise that are not accounted for. From Figure 3 we see that both vibration amplitudes and variances are larger when measured from the rotating side of the pinion and thus probably more likely to contain information regarding the oxygen blow process than the vibration measured from the fixed side.

B. Final Measurement Systems

The main objective of this research was to design a measurement system for research purposes which is able to measure mechanical vibration from the shaft of the BOF in three directions. The system should operate autonomously and store the measurement signals in its own memory that is unloaded at most once a day. Because the transfer of electric energy to the rotating shaft is difficult, the power supply of the measuring equipment is provided by batteries, which are replaced once a day or less often.

Based on the pre-measurements, the measurement equipment was decided to be mounted on the rotating part of the shaft, *i.e.*, to the trunnion pin. For this purpose, special housings were designed for the measuring equipment and its power supply, and these were manufactured out of ABS plastic by 3D printing. The housings were attached to the flange of the free end of the BOF 1 with the help of super magnets. In addition, it was decided that the audio measurements are recorded using a separate measurement equipment. The clocks of these two equipments were synchronized at the same set time.

C. Vibration Measurement System

The equipment designed for the vibration measurement of the BOF is shown in Figures 4 and 5. The equipment includes two housings, a CompactRIO data logger and its modules, a USB hard disk, a triaxial accelerometer, a 2-axis inclination sensor, cabling, fixing bolts, and eight power supplies. The 3D printed housing is mounted on the outer ring of the end flange of the vessel trunnion pin. X-, Y-, and Z-directions of the accelerometer are aligned with the coordinate system defined on the bottom-left section of Figure 4. X- and Y-directions are horizontal and vertical, respectively, and perpendicular to the trunnion pin of the vessel. Z-direction is horizontal and parallel to the trunnion pin. Due to space restrictions, the final setup location of both housings had to be moved clockwise a distance of one bolt when compared to Figure 4.

The measurement data logger is a combination of National Instruments CompactRIO product family devices. The system uses a base plate (cRIO-9113 chassis) having four slots for I/O-modules. The real-time controller unit (cRIO-9024) has 800 MHz processor, 4 GB non-volatile storage, 512 MB of DDR2 memory, and a USB host port. Analog IEPE input module (NI-9234) is used for three-channel acceleration measurements, analog voltage input module (NI-9215) for inclination sensor measurements, and solid-state relay

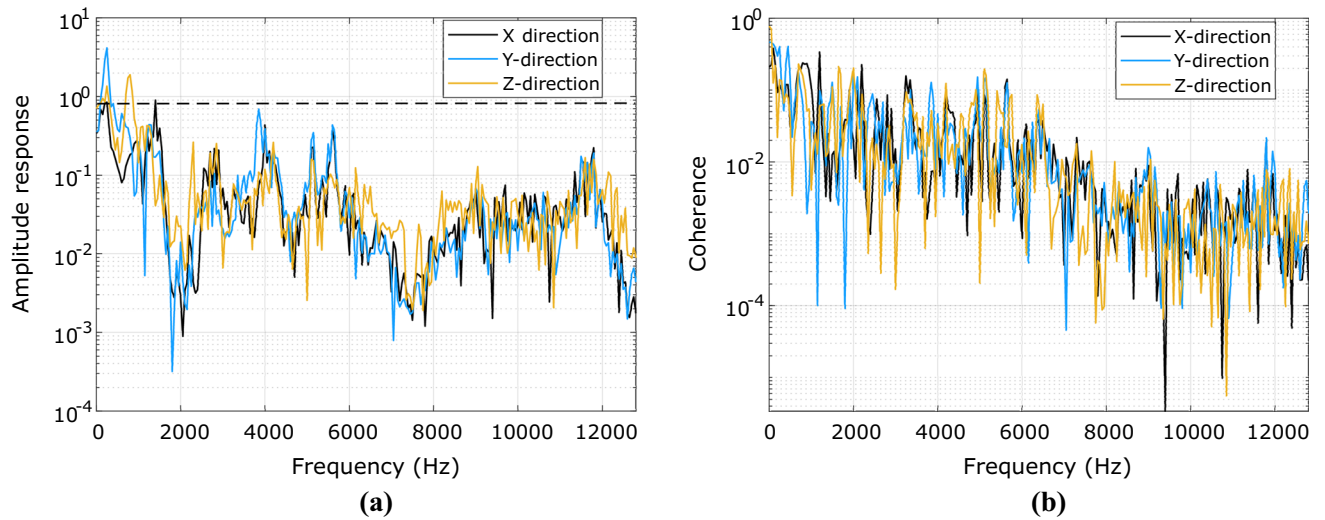


Fig. 2—The estimated (a) amplitude responses and (b) coherences from all measurement directions. The dashed line in (a) shows a gain of 1, and thus any values below it implies that attenuation has occurred.

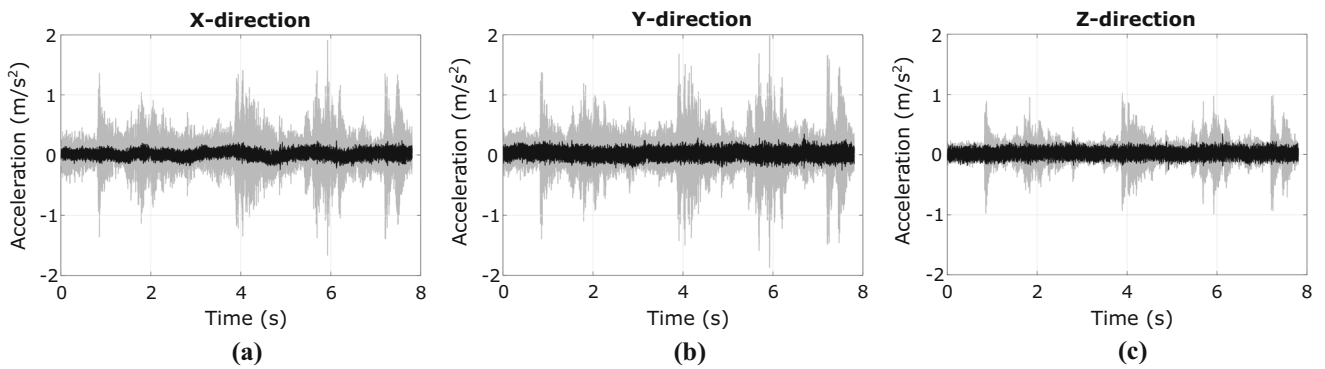


Fig. 3—The signal segments that were used in estimating the transfer functions and coherences. Gray signals are from the rotating side and black ones from the fixed side and (a) is X-direction, (b) is Y-direction, and (c) is Z-direction.

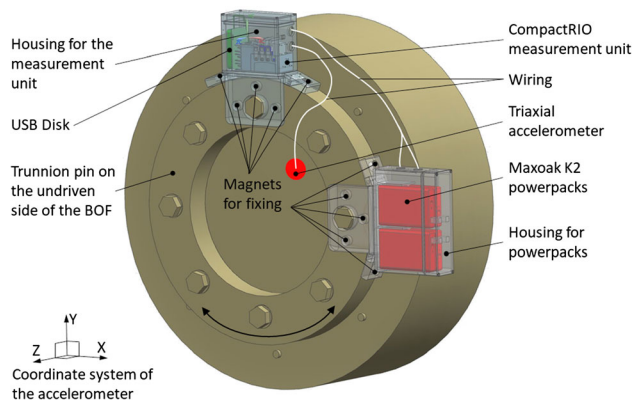


Fig. 4—Configuration of the measurement system for the vibration measurements.

digital output module NI-9485 for power supply control. The controller was programmed using LabVIEW software.

In addition, the measuring equipment consists of a changeable USB hard drive (HP My Passport Ultra 2 TB), a power switch, wirings, and fasteners. ABS plastic 3D printed parts are fixed to each other with M5 and M6 bolts. In the power supply housing, there is a place for four Maxoak K2 power supplies. In both housings, neodymium super magnets of 27 kg holding force are glued with epoxy adhesive to the 3D printed parts. Super magnets hold the housings in the end flange in the radial and axial directions. The device housings without the covering plates are shown in Figure 6.

The type of the triaxial accelerometer is MMF KS943B100 and its nominal sensitivity is 100 mV/g in all axis. Linear (± 3 dB) frequency range is from 0.5 Hz to 22 kHz (Z-axis). Mounting of the accelerometer to the trunnion pin of the BOF required special design work (see Figure 7). There are threaded pull-out holes (M20) on the end flange and one of these was utilized in accelerometer mounting. Head of an M20 bolt was machined flat and a threaded hole (M6) was drilled into it for the sensor mounting. The accelerometer was tightened to this bigger bolt head using a brass stud. The

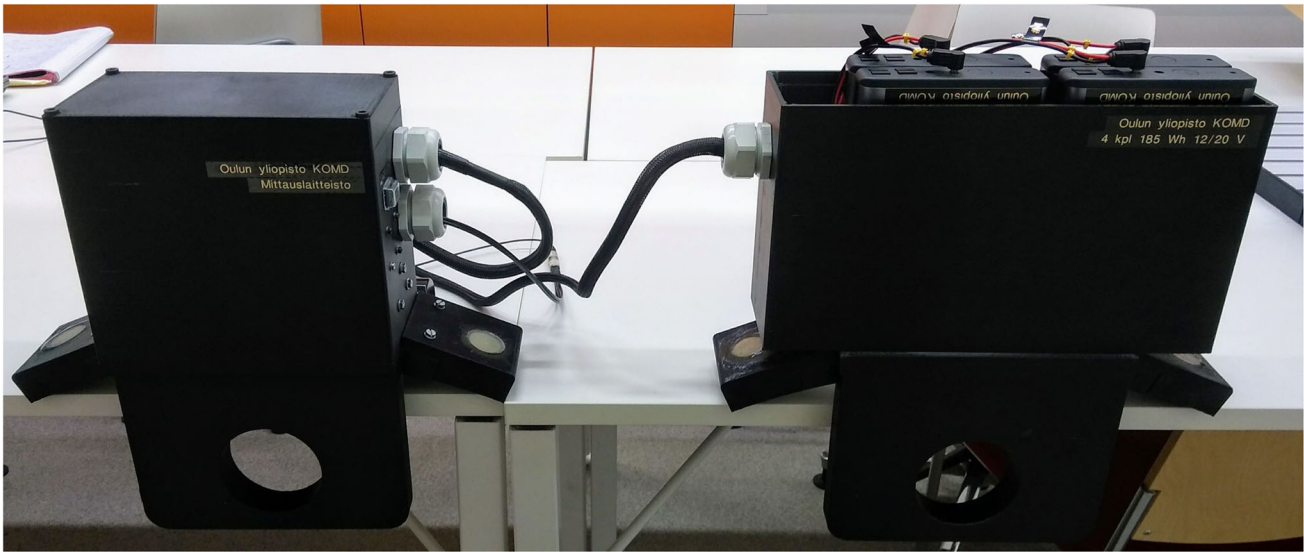
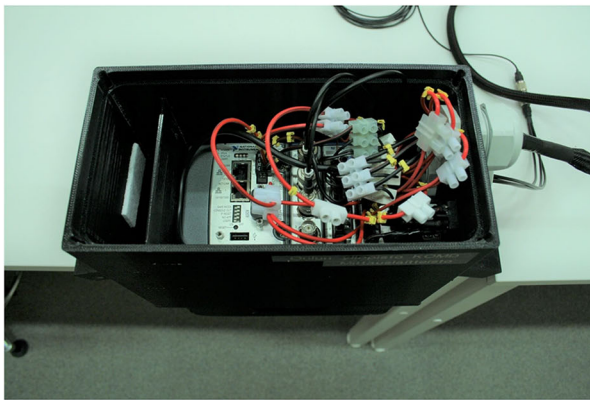
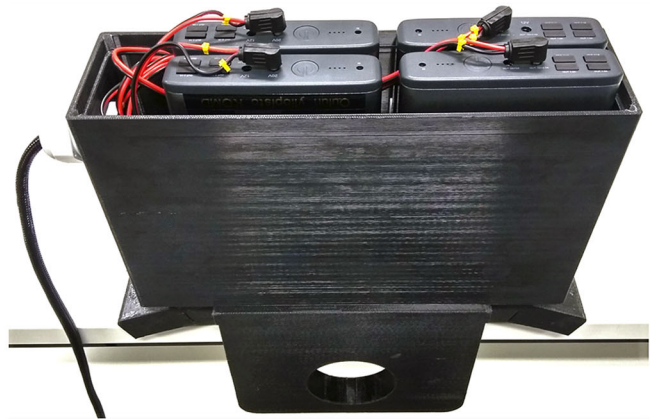


Fig. 5—3D printed housings of the vibration measurement system.



(a)



(b)

Fig. 6—Uncovered measurement device housing in (a) and power supply housing in (b).

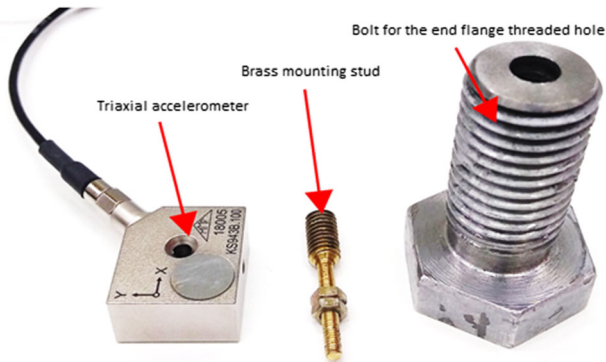


Fig. 7—Accelerometer and its special mounting accessories.

sensor position was adjusted so that its measuring directions were set to the horizontal and vertical direction as carefully as possible.

The power supply of the measurement equipment was carried out with Maxoak K2 uninterruptible power supply (UPS) devices of 185 Wh capacity. They can supply either 12 V or 20 V DC voltage. The power supplies have a timeout feature, which turns off the power supply after 30 seconds if the lower limit of the power consumption is not exceeded. For this reason, the power supplies were loaded with the help of power resistors (5 W 68 Ohm) and the NI-9485 relay control module so that the power supplies will not turn off during the measurements.

Four power supplies were installed at the same time, and they supply power to the measurement device alternately controlled by the relay control module. They should be able to carry out the power supply of the equipment together for about 2 days. After that, the power supplies have to be changed to charged ones. The circuit diagram of the vibration measurement system is shown in Figure 8.

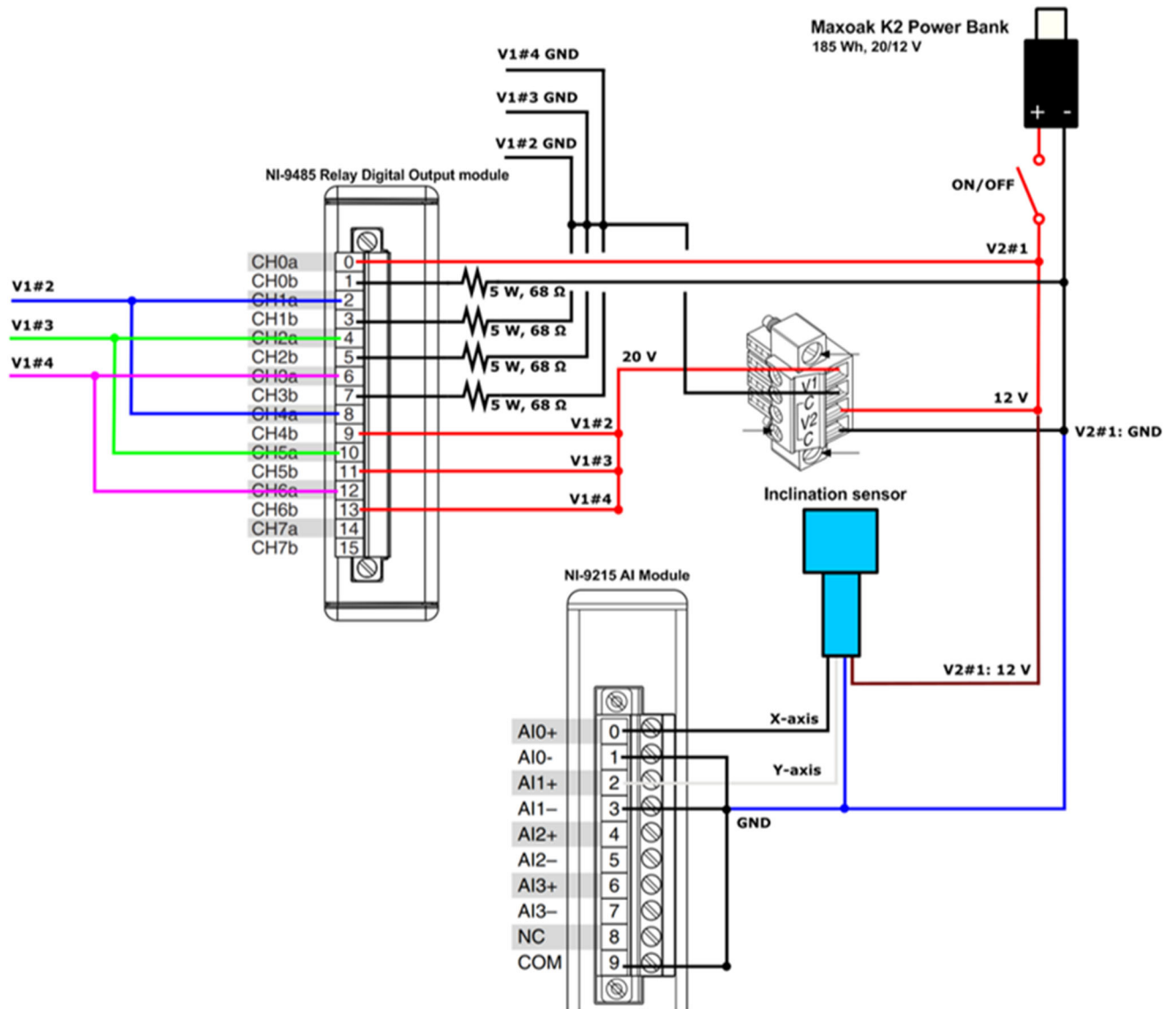


Fig. 8—Circuit diagram of the acceleration measurement system.

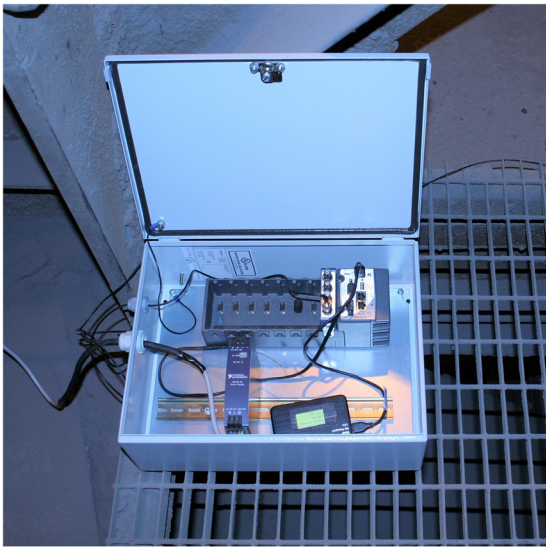
The measurement data were stored on external USB hard disks. The sampling frequency was 51.2 kHz, and the data were recorded simultaneously on three channels from the 3-axial accelerometer and on one channel from the inclination sensor. The measurement data accumulated at the speed 5.474 GB per hour, and this meant that the volume of the data that accumulated in seven days was about one terabyte.

D. Audio Measurement System

Audio measurements were carried out with another measurement system from the upper section of the BOF. The equipment includes an industrial microphone, a CompactRIO data logger with an analog input module, 24 V DC power supply, and a USB hard disk. This equipment was powered by mains supply.

The measurement data logger is a combination of National Instruments CompactRIO product family devices. The system uses a base plate (cRIO-9114 chassis) having eight slots for I/O-modules. The real-time controller unit (cRIO-9024) was similar to the controller of the vibration measurement system. An analog IEPE input module (NI-9234) was used for microphone data logging. The external USB hard drive (HP My Passport Ultra 2 TB) is also the same model that was used in the vibration measurement system. The controller was programmed using LabVIEW software. The CompactRIO equipment with the DC power supply and the USB hard drive was installed in a metallic sealed device housing (Figure 9).

The type of the microphone is GRAS 40PH, it is an array microphone with nominal sensitivity (at 250 Hz) 50 mV/Pa (± 2 dB). The microphone's sensitivity is calibrated to 47.70 mV/Pa. Linear (± 3 dB) frequency



(a)



(b)

Fig. 9—Housing of the audio measurement system in (a) and the microphone installed to its place above BOF 1 in (b). Arrow 1 in (b) shows a cover for the flux addition chute. Arrow 2 is a dust exhaust pipe from the flux addition chute. Arrow 3 shows the water-cooled off-gas hood and arrow 4 is a water pipe that connects to the mentioned water-cooling system.

range is from 10 Hz to 50 kHz. There is an integrated CCP preamplifier in the microphone and it requires a constant-current power, which was supplied by the CompactRIO module NI-9234.

The microphone was installed to a stand and protected with foam windscreen and metal mesh housing (see Figure 9). Also the cable was protected with a fireproof sock because sparking is possible in the measuring place.

The audio measurement data were stored on external USB hard disks by using the same sampling frequency 51.2 kHz as in the vibration measurements. Since only one channel data were recorded, the hard disk space was enough for the whole month.

III. RESULTS AND DISCUSSION

A. Pre-processing

The pre-processing steps were the following:

- a. Separation of the blows from the almost continuous data stream, a total of 286 blows were collected which had both audio and vibration recordings.
- b. Finding the exact start times of the oxygen blows.
- c. Calculation of spectrograms for a period of 1200 seconds from start of a blow.

The vibration directions are treated separately to see if there are any notable differences between them and if some directions are more interesting related to the BOF process.

The 1-minute-long binary files were combined to longer files using the blow start and end times provided by SSAB. Five minutes of data were included to the file before the start time and 10 minutes of data after the stop time. These precautions were taken because the

clocks of the data loggers and SSAB's automation system were noticed to be asynchronous. The data from the inclination sensor were also discarded from these long files, as its recording had failed. The inclination data were correctly recorded for less than 23 minutes after which the data froze to a constant value. This was probably caused by an error in the LabView program, as the inclination sensor was tested after the measurement campaign, and it was still functional.

At this point, RMS (root mean square) values of the vibration and audio signals were calculated from several frequency bands in 1-s interval and the ones filtered to 3–20 Hz were used in finding the exact start times of the oxygen blows (to approximately 1 second of accuracy). This was visible as a rise in the vibration and audio levels. This semiautomatic procedure was very effective at locating the oxygen blows in the audio signals, but sometimes failed in the vibration signals because there was more activity there even before the oxygen blow. A manual check was thus conducted to verify that the correct duration of the oxygen blow was found.

Next, it was feasible to do a more accurate frequency analysis for the whole duration of the oxygen blows. Discrete Fourier transforms (DFT) were computed using 1-s windows (number of samples in a transform: $N = 51200$) for a total of 1200 seconds for each blow, which was the maximum recorded length of an oxygen blow. Before the DFT, the 1-second samples were windowed with a smooth window function whose rise and fall times were 0.1 seconds.

The spectrograms contain a huge amount of information. We visualize this using one example blow, number 46 on our list. The length of oxygen flow was 1069 seconds for this particular blow. Figures 10 (a) and (b) show the spectrograms from the acceleration measurements of X-direction in the frequency range

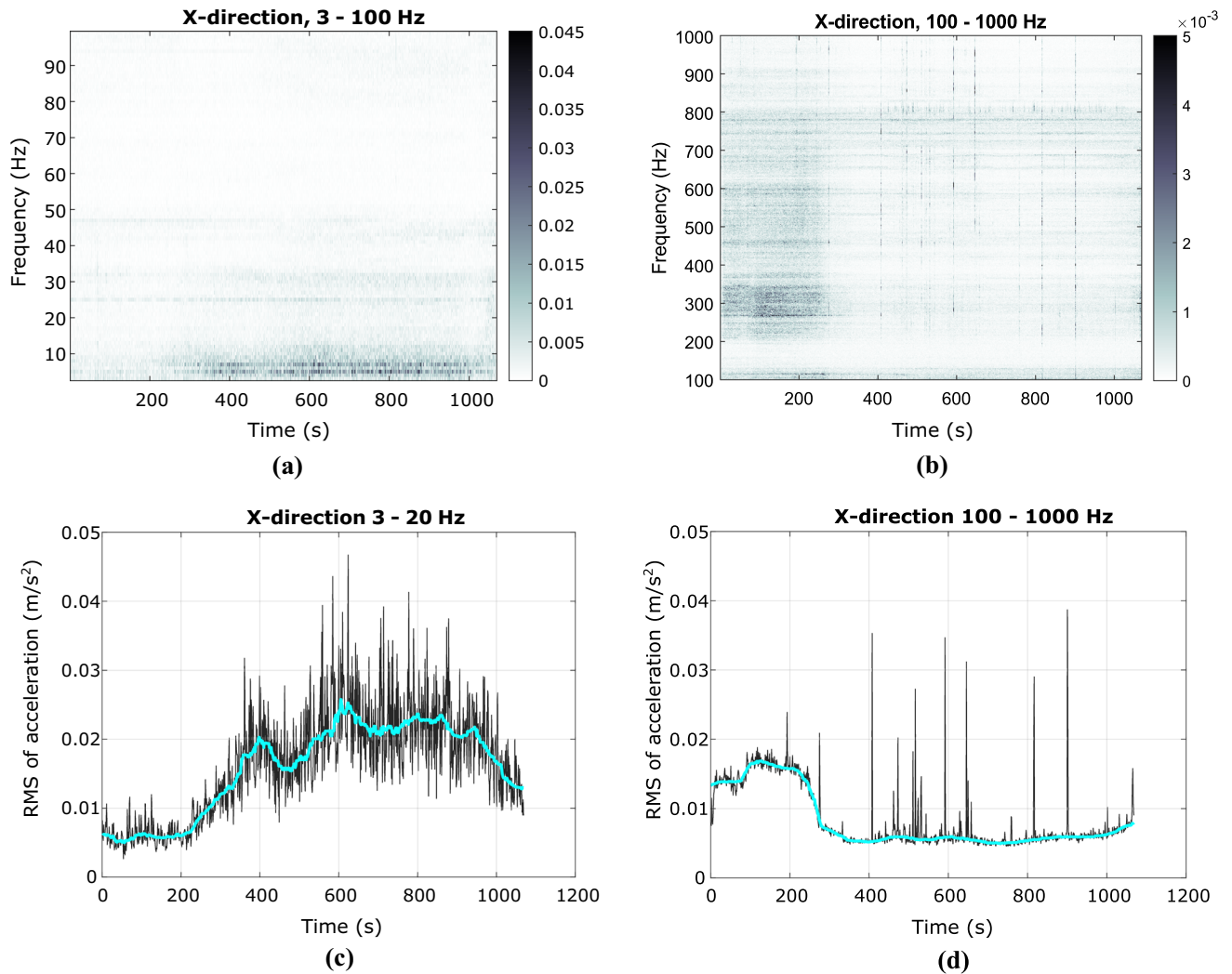


Fig. 10—Spectrograms in the range (a) 3–100 Hz and (b) 100–1000 Hz and RMS signals in the range (c) 3–20 Hz and (d) 100–1000 Hz and also median filtered from the X-direction acceleration measurements of the blow no. 46.

3–100 Hz and 100–1000 Hz and (c) and (d) two RMS signals, which were produced after filtering to the ranges 3–20 Hz and 100–1000 Hz and their median filtered versions (plotted with a bright color) with window length 51 seconds. From the RMS signals we see that the low-frequency vibration increases toward the end of the blow, whereas the vibration in the range 100–1000 Hz is significant only during the first 280 seconds of the blow. The spectrogram in the range 3–100 Hz shows that most of the low-frequency vibration occurs at 5 and 7 Hz. In the spectrograms from the range 3–100 Hz, the acceleration amplitudes are shown with colors from 0 to 0.045 m/s^2 and in the spectrograms from the range 100–1000 Hz the acceleration amplitudes are shown with colors from 0 to 0.005 m/s^2 . All bigger values get the same color as the maximum value. Some of the short duration bursts caused vibration amplitudes up to 1.2 m/s^2 , but it would make the pictures very non-informative if these were allowed to affect the color scales. It is also notable that there exists

a lot of vibration information in the higher frequencies up to the Nyquist frequency 25.6 kHz, but we choose not to analyze them in detail in this study.

Figures 11 and 12 show the corresponding calculations from Y- and Z-directions, respectively. The most significant difference between the directions is that the low-frequency vibration in the Y-direction is almost stationary during the whole blow. The low-frequency vibration in the Z-direction occurs mostly at 8–10 Hz and around 26 Hz and increases toward the end of the blow. The RMS signals from the range 100–1000 Hz are almost identical for all the directions.

Finally, Figure 13 shows corresponding calculations from the audio measurements. Even though not shown, we mention here that the audio amplitudes decrease so fast with increasing frequency that the spectrogram with the whole range 3–25600 Hz would look very flat and uninteresting. The RMS signal from the range 3–20 Hz resembles quite closely the ones from the vibration X- and Z-directions, except that there is an additional

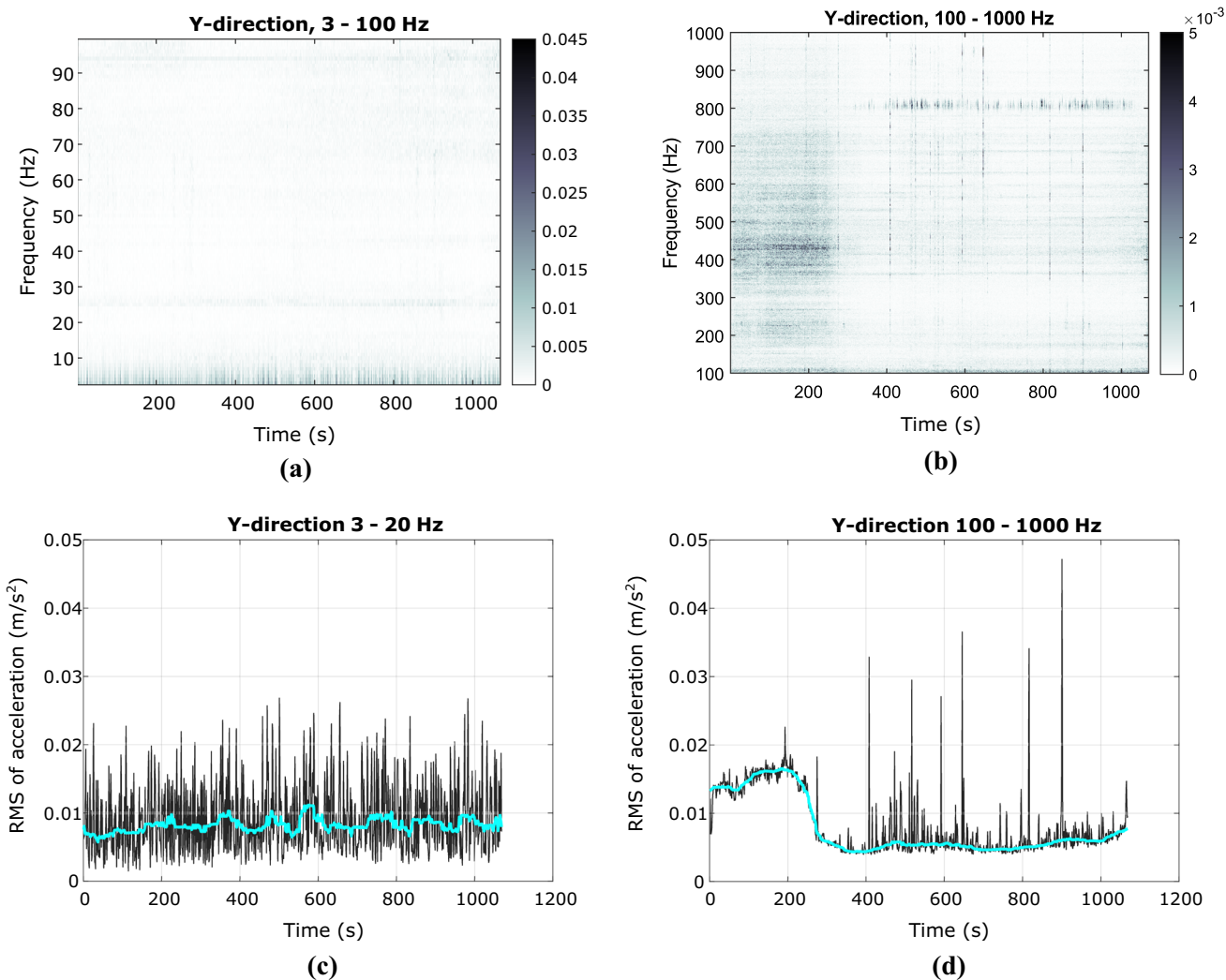


Fig. 11—Spectrograms in the range (a) 3–100 Hz and (b) 100–1000 Hz and RMS signals in the range (c) 3–20 Hz and (d) 100–1000 Hz and also median filtered from the Y-direction acceleration measurements of the blow no. 46.

bump occurring at 100 seconds after the start of the oxygen flow and the RMS of audio data diminishes quickly near the end of the blow. The most significant low-frequency amplitudes occur around the frequencies 6 and 12 Hz. The RMS signal from the range 100–1000 Hz is very similar to the vibration RMS signals, except that there is an additional bump near the end.

Off-gas temperature and lance height of the blow no. 46 are shown in Figures 14(a) and (b). The zero point of the lance height is a certain fixed height inside the converter. Comparing Figure 14(a) and (b) to the previous figures, it seems plausible to suggest that especially the low-frequency (3–20 Hz) audio data correlate to some extent with the off-gas temperature and the lance height possibly correlates with the 100–1000 Hz frequency range audio and vibration data during the first half of the blow. The shape of the measured audio intensity in Reference 12 is very similar

to our measurements. The measured audio intensities in Reference 11 also contain the characteristic drop near the end of the blow.

B. Correlations Between Measurements and Process Data

As mentioned in the previous section, there might be some correlation between the off-gas temperature and the measured low-frequency audio data. It is known that the off-gas temperature itself correlates mainly with the decarburization rate. It is, however, not clear what exactly causes the drop in the temperature at roughly 200–400 seconds in Figure 14(a). This is a consistent feature between heats, and it is also consistently visible in the audio RMS data from the range 3–20 Hz as demonstrated in Figure 13(a). We also note that this drop is similarly visible at 2 minutes of mark in the audio intensity Figure 1 of Reference 12. A drop is also visible in the CO percentage content of the measured off-gas in Figure 1 in Reference 19 (also published as

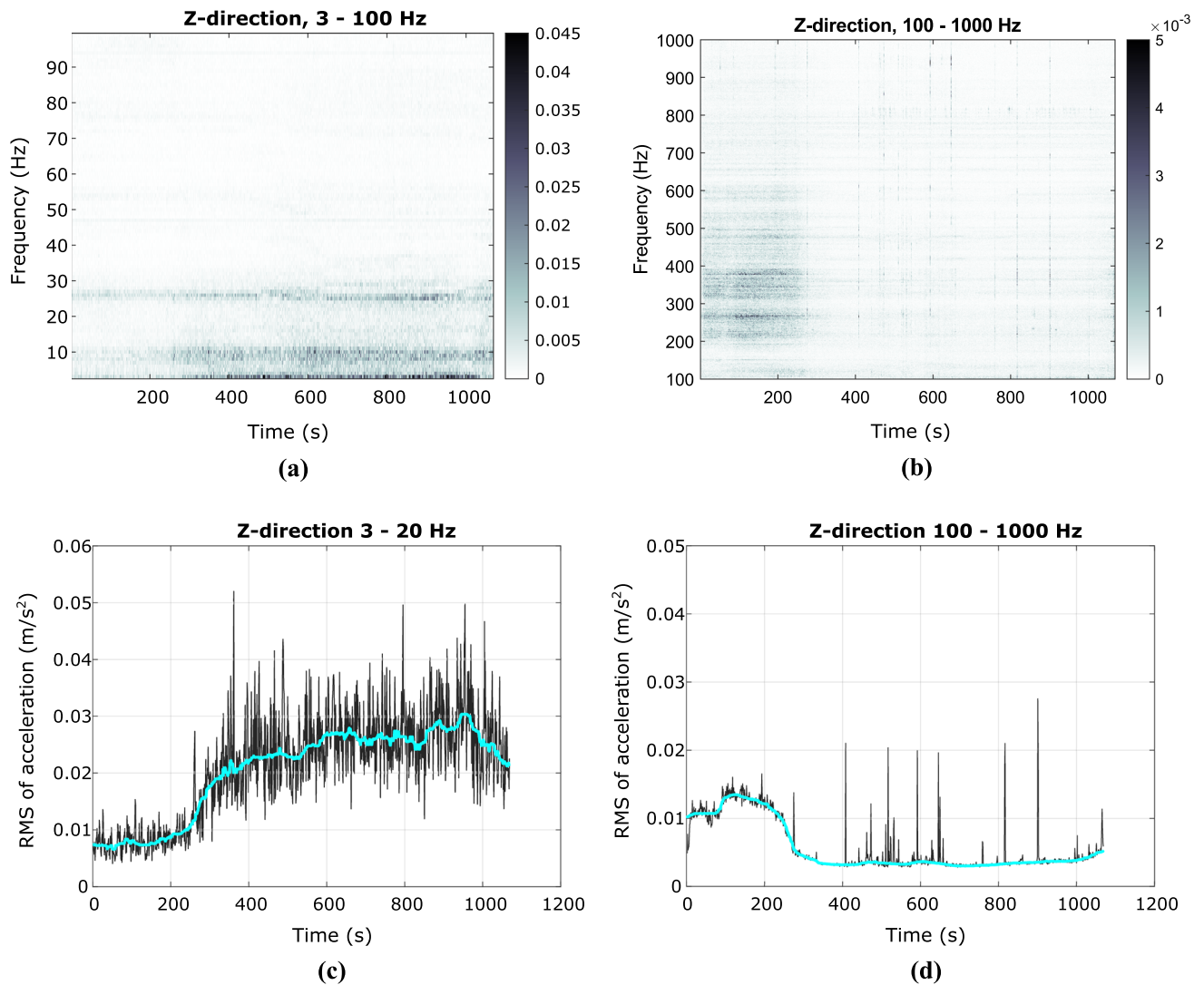


Fig. 12—Spectrograms in the range (a) 3–100 Hz and (b) 100–1000 Hz and RMS signals in the range (c) 3–20 Hz and (d) 100–1000 Hz and also median filtered from the Z-direction acceleration measurements of the blow no. 46.

Figure 9.16 in Reference 1) at about 3 minutes of mark and similarly in the CO percentage content of the off-gas produced by a dynamic model of a BOF at about 1.5-min mark in Reference 20. The correlation of one numerically predicted decarburization rate curve and the measured CO content of the off-gas is also visualized in Reference 21.

Another correlation was observed between vibration and audio measurements in the range 100–1000 Hz and lance height. This might be related to the effect of lance height on the behavior of the cavity. Molloy^[22] defined three cavity modes: (1) dimpling mode, which denotes small surface depression and is typical for a low jet velocity and/or high lance height, (2) splashing mode, which is characterized by a shallow cavity and ejection of a large amounts of droplets from the outer rim of the cavity, and (3) penetrating mode, which denotes a deep penetration accompanied by a reduction in the outwardly directed ejection of droplets and is typical for a

high gas jet velocity and/or low lance height. Using this terminology, decreasing the lance height might change the cavity mode from splashing to penetrating mode. In Reference 8, changes in the audio spectra are recorded when the cavity changed from splashing to penetrating. The main change in the in the audio spectra was the increase in amplitude roughly in the range of 500 to 2500 Hz.^[8]

To study these propositions, we wanted to calculate correlation coefficients from the large data collected in this study. Several heats were excluded from this analysis since they had abnormal features that would have clearly affected some of the results badly. These features were stoppages in the oxygen flow during the heat, stoppages in the audio data recording (these were caused by the audio measurement system booting once per day), and also unexpected sudden big shifts in the lance height profile. After this pruning, there remained 275 heats. We use the following terms adapted from

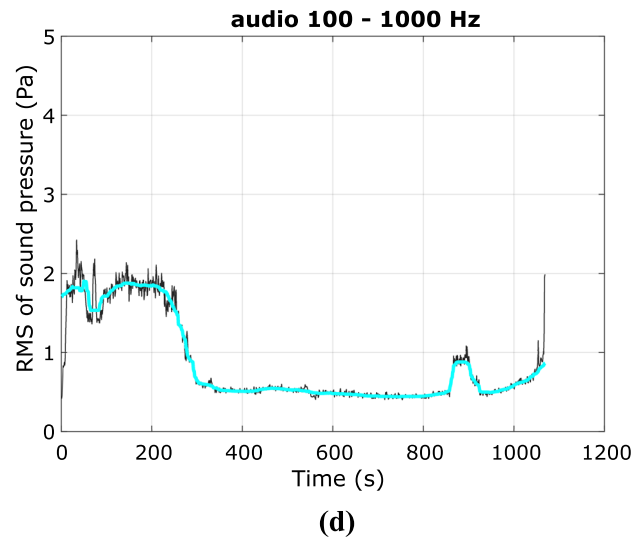
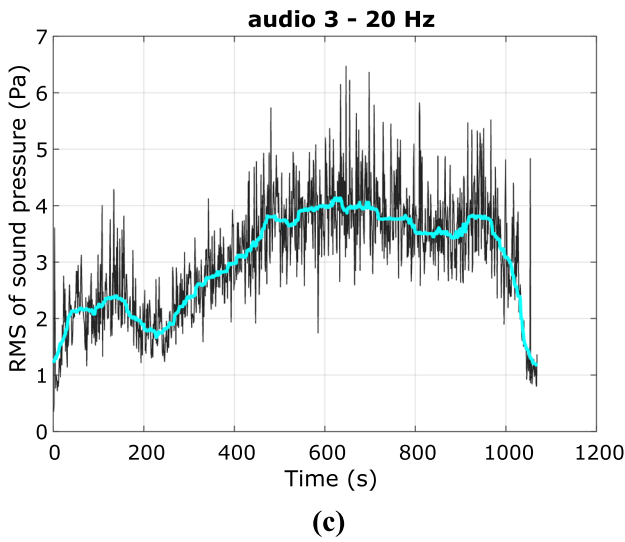
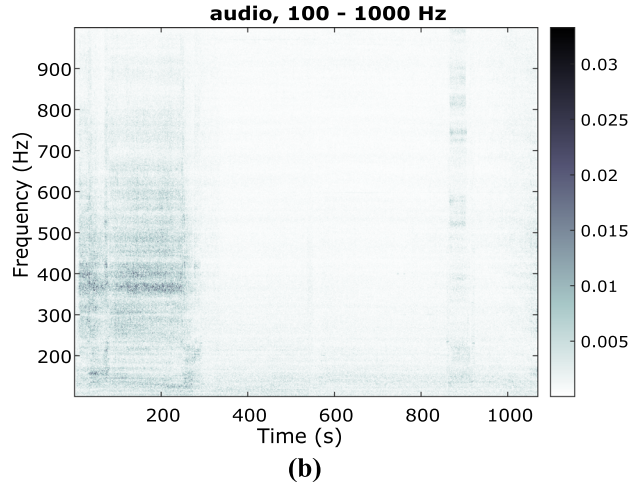
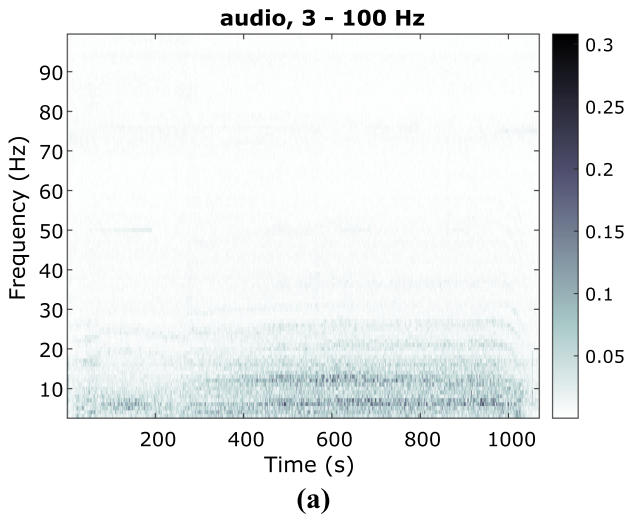


Fig. 13—Spectrograms in the range (a) 3–100 Hz and (b) 100–1000 Hz and RMS signals in the range (c) 3–20 Hz and (d) 100–1000 Hz and also median filtered from the audio measurements of the blow no. 46.

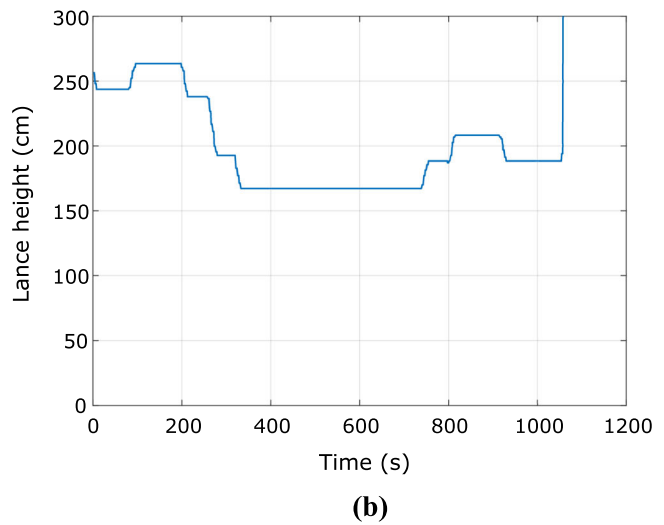
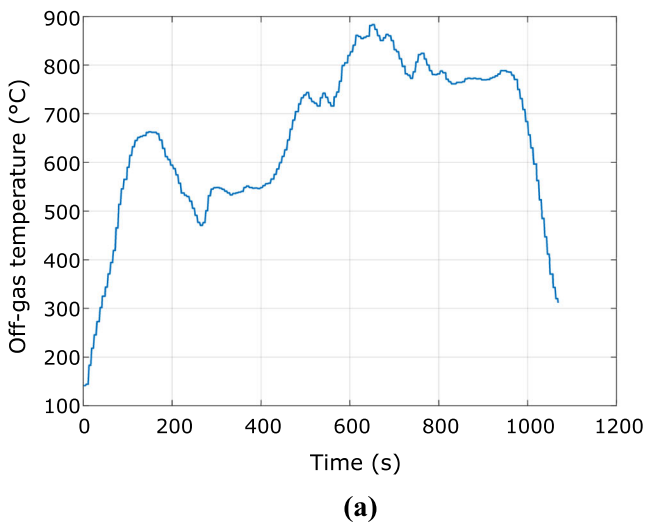


Fig. 14—(a) Off-gas temperature and (b) lance height of the blow no. 46.

Reference 23 to describe the size of correlation: 0.90 to 1.00 is very high positive correlation, 0.70 to 0.90 is high positive, 0.50 to 0.70 is moderate positive, 0.30 to 0.50 is low positive, and 0.00 to 0.30 is negligible.

As mentioned in the pre-processing section, the starting times of the heats (= the start of the oxygen flow) for vibration and sound measurements had to be determined experimentally from the data. For the process data that was gathered from the automation system of SSAB, we could simply limit our attention to the time interval during which the oxygen flow was greater than zero. This means that the vibration/sound time series have been synced with the process data at roughly 1 seconds of accuracy.

Figure 15(a) shows the correlation coefficients calculated separately for all 275 heats between audio RMS from 3 to 20 Hz and off-gas temperature for the whole duration of each oxygen blow and in (b) this linear regression is visualized for the whole dataset. Black values in (a) are calculated using the audio RMS values and bright values using the median filtered audio RMS values. The mean for the 275 correlation coefficients in (a) is high positive at 0.846, the median is 0.859, and the standard dev. is 0.059 when the smoothed RMS values are used. The sample correlation from the whole dataset (b) is also high positive at 0.823. Its 95 pct confidence interval is also shown in Table II. The interval is calculated assuming normally distributed deviations from the linear regression fit (plotted line).

Figure 16 shows the same calculations between the X-direction acceleration RMS from 3 to 20 Hz and off-gas temperature. The mean for correlation coefficients in (a) when the smoothed RMS values are used is 0.620, the median is 0.660 and the standard dev. is 0.174. This is moderate positive correlation. The correlation from the whole dataset (b) is also moderate positive at 0.580. Its confidence interval is shown in Table II.

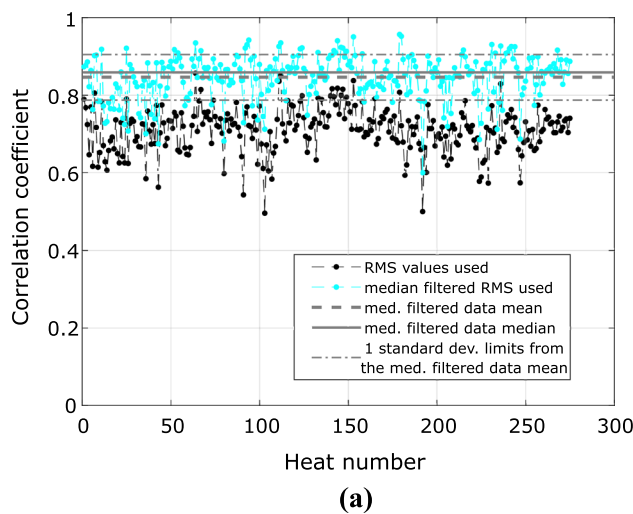


Figure 17(a) shows the correlation coefficients from all 275 heats between audio RMS from 100 to 1000 Hz and lance height from the time period 20–600 s since the start of the oxygen blow. Again, the black values in (a) are calculated using the audio RMS values and the bright values using the median filtered audio RMS values. The mean correlation coefficient of the 275 heats in (a) using the median filtered audio data is very high positive at 0.946, the median is 0.959, and the standard dev. is 0.046. Also, even without the median filtering the correlations seem to be good. There are, however, two outliers for which the correlation is only about 0.6 even with median filtering the audio data. These are heat numbers 4 and 94 and we will look at them in more detail shortly. The sample correlation from the whole dataset in (b) is high positive at 0.821. Its confidence interval is shown in Table II.

Figure 18 shows the same calculations between the X-direction acceleration RMS from 100 to 1000 Hz and lance height. The mean for the correlation coefficients in (a) when using median filtered acceleration data is very high positive at 0.958, the median is 0.970, and the standard dev. is 0.049. The correlations for the unfiltered vibration data are much worse on average, most probably due to the noise as seen in Figure 10(d), Figures 11(d), and 12(d). Again, the heats 4 and 94 are clear outliers for the median filtered data, but also heat 182 is more than three standard deviations below the mean. The sample correlation from the whole dataset in (b) is high positive at 0.823. Its confidence interval is shown in Table II.

To make sure that the normality assumptions used in the calculations of the correlation coefficients and their confidence intervals did not cause erroneous results, we repeated the correlation analysis using the non-parametric method called bootstrapping.^[24] Figure 19 shows the distributions of the correlation coefficients calculated using 20000 repeats of bootstrapping for each case.

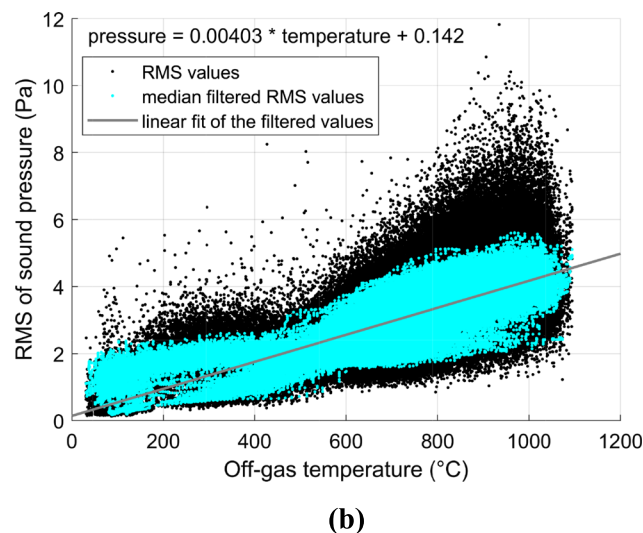


Fig. 15—(a) Correlation of audio RMS from 3 to 20 Hz and off-gas temperature for the whole duration of the oxygen blow for each heat separately and (b) the linear regression visualized for the whole dataset. The correlation coefficient for the median filtered data in (b) is 0.823 and its confidence intervals are shown in Table II.

Table II. Sample Correlation Coefficients Calculated from the Whole Datasets (= Data from 275 Heats Combined), Their Confidence Intervals Assuming Normally Distributed Deviations of the Dependent Variable as Well as Medians of the Bootstrapped Distributions and Their Confidence Intervals

Dependent and Independent Variables	Sample Correlation Coefficient r	95 pct Confidence Interval of r Assuming Normally Distributed Deviations	Median of the Bootstrapped Distribution of r	95 pct Confidence Interval of the Bootstrapped Distribution of r
Smoothed audio RMS 3–20 Hz vs off-gas temperature	0.8229	0.8217 – 0.8241	0.8229	0.8219 – 0.8239
Smoothed X-dir. vibr. RMS 3–20 Hz vs off-gas temperature	<u>0.5798</u>	<u>0.5773 – 0.5822</u>	<u>0.5798</u>	<u>0.5770 – 0.5826</u>
Smoothed Y-dir. vibr. RMS 3–20 Hz vs off-gas temperature	<i>0.0149</i>	<i>0.0112 – 0.0186</i>	<i>0.0149</i>	<i>0.0105 – 0.0193</i>
Smoothed Z-dir. vibr. RMS 3–20 Hz vs off-gas temperature	<u>0.6143</u>	<u>0.6119 – 0.6166</u>	<u>0.6143</u>	<u>0.6119 – 0.6166</u>
Smoothed audio RMS 100–1000 Hz vs lance height for the period of 20 – 600 s	0.8205	0.8189 – 0.8221	0.8205	0.8191 – 0.8219
Smoothed X-dir. vibr. RMS 100–1000 Hz vs lance height for the period of 20 – 600 s	0.8225	0.8209 – 0.8241	0.8225	0.8212 – 0.8239
Smoothed Y-dir RMS 100–1000 Hz vs lance height for the period of 20 – 600 s	0.8073	0.8056 – 0.8090	0.8073	0.8059 – 0.8087
Smoothed Z-dir RMS 100–1000 Hz vs lance height for the period of 20 – 600 s	0.8213	0.8197 – 0.8229	0.8213	0.8200 – 0.8226

The values are highlighted according to these categories: 0.90 to 1.00 is very high positive correlation, 0.70 to 0.90 is high positive (Bold), 0.50 to 0.70 is moderate positive (Underline), 0.30 to 0.50 is low positive, and 0.00 to 0.30 is negligible (Italic).

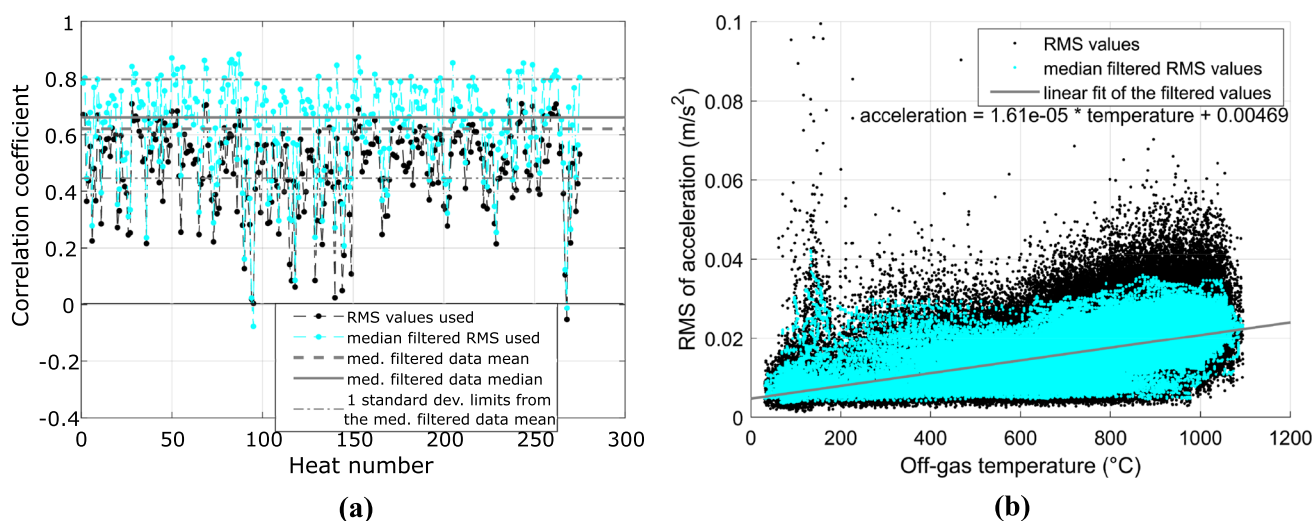


Fig. 16—(a) Correlation of X-direction vibration RMS from 3 to 20 Hz and off-gas temperature for the whole duration of the oxygen blow for each heat separately and (b) the linear regression visualized for the whole dataset. The correlation coefficient for the median filtered data in (b) is 0.580 and its confidence intervals are shown in Table II.

The medians of these distributions are taken to represent the correlation coefficients and the confidence intervals can also be read from these distributions. These numbers are also represented in Table II.

We see that the sample correlation coefficients are exactly the same as the medians of the bootstrapped distributions to 4 decimal accuracy. The confidence intervals differ but not very much. We also note that the correlations for vibrations of Y- and Z-directions are very similar to the X-direction except for the smoothed

vibrations RMS in the Y-direction RMS 3–20 Hz vs off-gas temperature, for which the correlation is negligible. But even for this case, the 95 pct confidence intervals do not contain 0, which means that the existence of this negligible correlation cannot be ruled out.

Figures 20(a) and (b) show the audio RMS from 100 to 1000 Hz of the heats 4 and 94 and their corresponding lance height profiles in (c) and (d) and also X-direction vibration RMS from 100 to 1000 Hz in (e)

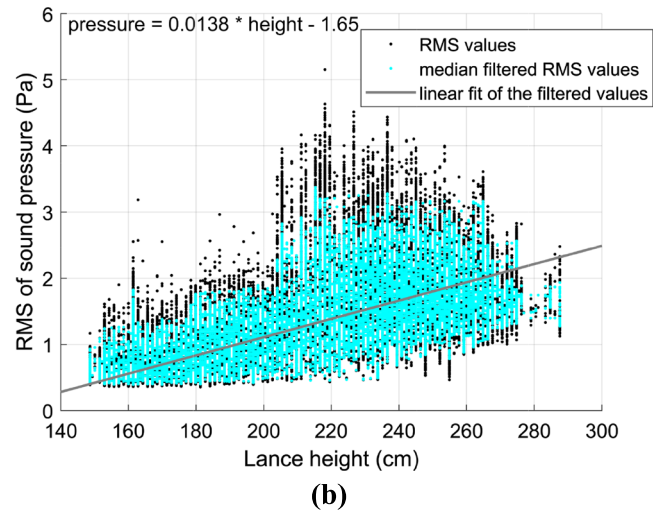
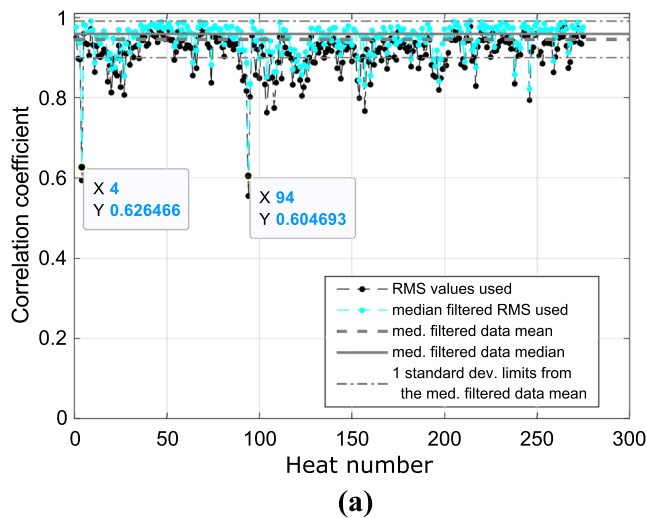


Fig. 17—(a) Correlation of audio RMS from 100 to 1000 Hz and lance height for the period of 20–600 s from the beginning of oxygen blow for each heat separately and (b) the linear regression visualized for the whole dataset. The correlation coefficient for the median filtered data in (b) is 0.821 and its confidence intervals are shown in Table II.

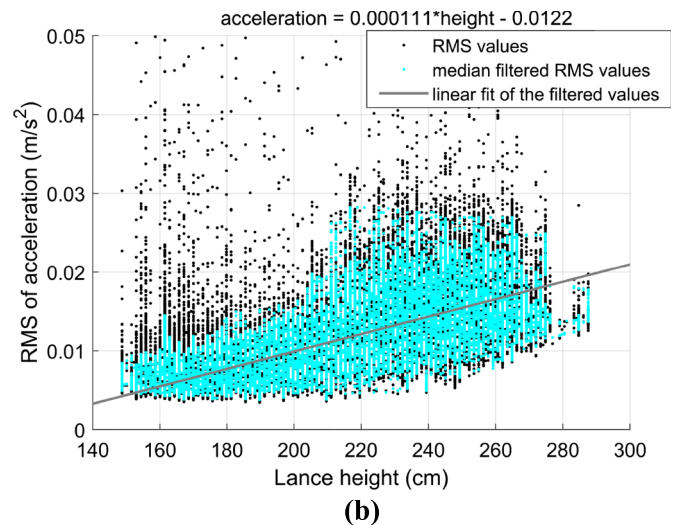
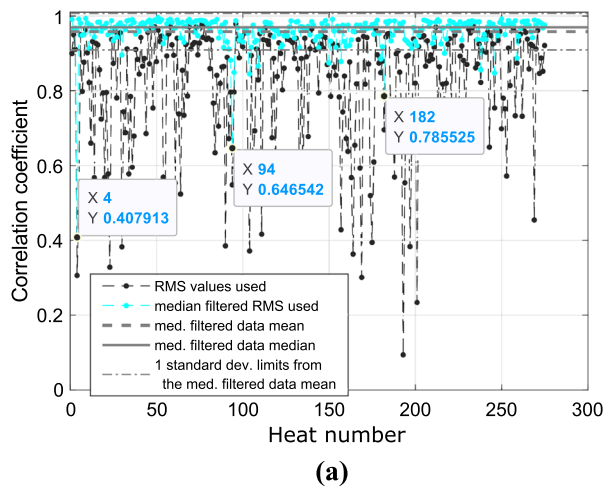


Fig. 18—(a) Correlation of X-direction vibration RMS from 100 to 1000 Hz and lance height for the period of 20–600 s from the beginning of oxygen blow for each heat separately and (b) the linear regression visualized for the whole dataset. The correlation coefficient for the median filtered data in (b) is 0.823 and its confidence intervals are shown in Table II.

and (f). From about 300 s onwards both of these heats have increasing activity in this frequency range which is typically absent in other heats. This frequency range for audio signals was studied in slopping control in Reference 7, but the interpretation of their results proved to be inconclusive. The BOF process consists of three decarburization regimes: onset, linear decrease (*i.e.*, the main decarburization), and run out.^[25]

Correspondingly, the initial part of the heat is characterized by strong foam generation, which is followed by a virtually steady-state foam level during main decarburization until the foam starts to collapse as a result of the diminishing decarburization rate in the final part of the heat.^[26] In view of these considerations, it is interesting to note that the frequency range of

100–1000 Hz correlates well with the changes in lance height in the initial part of the heat, which is conducted with a high lance position, but not in the final part of the heat, when the lance is lifted again. It is thus likely that this frequency range is associated with the droplet generation mechanism driving the generation of the metal–gas–slag foam.

Figures 21(a) through (c) show the X-direction vibration, Z-direction vibration, and audio RMS from 100 to 1000 Hz from the heat 182 and (d) shows the corresponding lance height profile. Again, there is untypical activity in this frequency range from about 400 seconds onwards which could be related to abnormal slag formation or possibly slopping. Since the oxygen is normally supplied with quite a steady rate, this

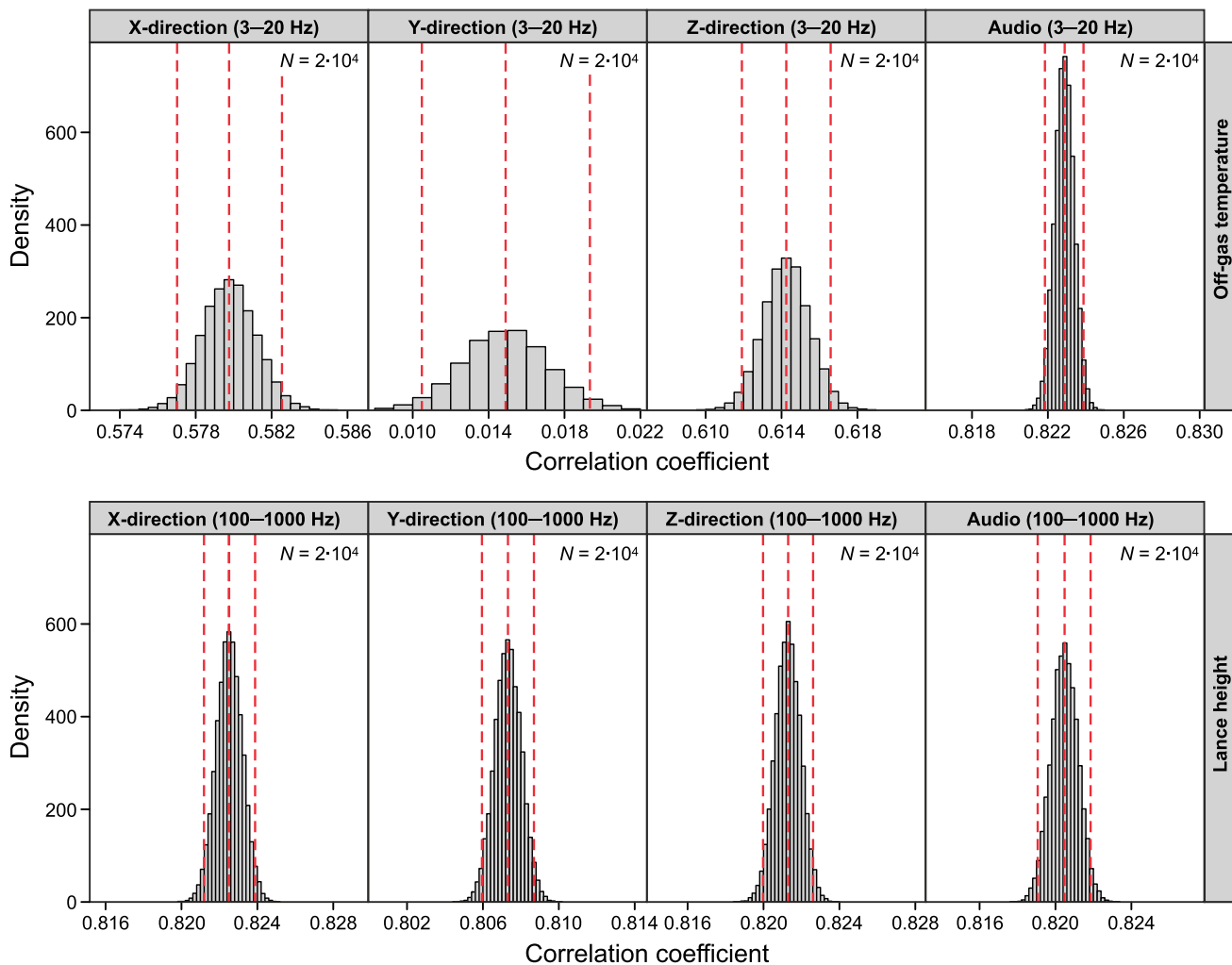


Fig. 19—Bootstrapped distributions of the correlation coefficients from all of the previous cases and also from Y- and Z-direction acceleration measurements. Their medians and 95 pct confidence intervals are highlighted.

timing matches the observation in Reference 9 that slopping typically occurs when 30–40 pct of oxygen is supplied. Unfortunately, we do not have any confirmed recordings of slopping events from the measurement period. Figures 22(a) through (c) show the X-direction vibration, Z-direction vibration, and audio RMS from 3 to 20 Hz from the heat 182 and (d) shows its off-gas temperature. The shape of the off-gas temperature is fairly typical although also a bit higher during the first half compared to heat 46 in Figure 14. The low-frequency vibration RMS in the X- and Z-directions and audio RMS increase during the heat. We do not see such pronounced steps in the measurements during the first half as we did with heat no. 46. It should be noted that heat no. 182 was charged only with hot metal with no scrap.

Figure 23(a) and (b) show the audio RMS from 3 to 20 Hz of the heats 4 and 94 and their corresponding off-gas temperatures in (c) and (d) and also X-direction vibration RMS from 3–20 Hz in (e) and (f). Here, we can see the pronounced step in the audio RMS time

series as we did with heat 46 in Figure 13. This is less pronounced with the X-direction vibration RMS time series for heat 4 and very different for heat 94. In (f) the vibration RMS increases only during the latter half of the heat. The off-gas temperatures for all three outlier heats reach 1000 °C, which is over 100 °C hotter than with the example heat no. 46. But from the compiled data in Figures 15 and 16 we see that some heats have reached nearly 1100 °C, so the discussed outliers were not the hottest heats in the dataset, though heat no. 182 came quite close.

C. Application of the Results

Many predictive models have been developed between some input and output parameters of the BOF process. For example, a BOF process control system based on an off-gas analyzer (a mass spectrometer) was presented in Reference 27. The gas data were utilized to control the amount of oxygen retained in the BOF by making lance height adjustments. Prediction of the endpoint

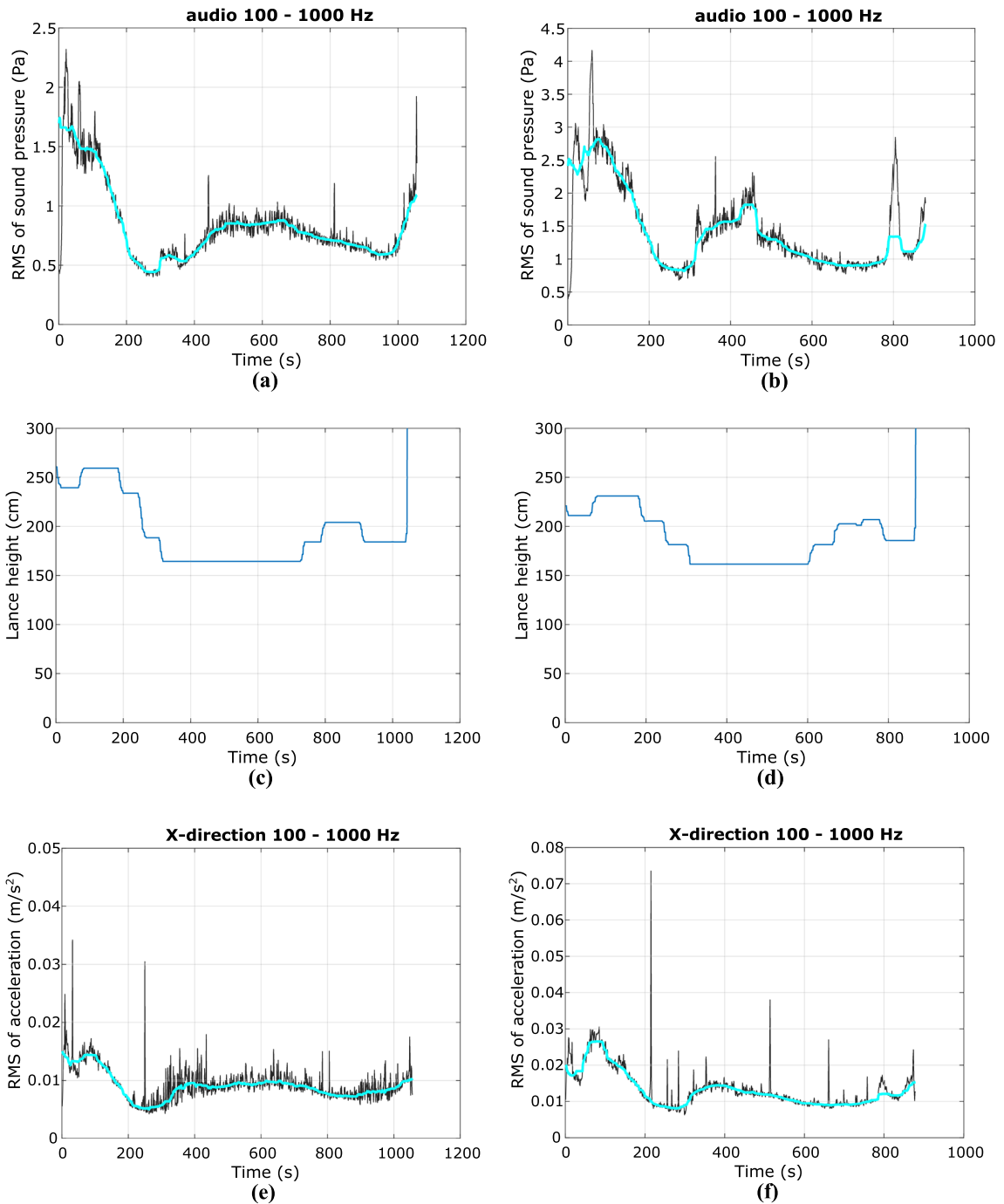


Fig. 20—The audio RMS from 100 to 1000 Hz of (a) heat 4 and (b) heat 94, lance height profile of (c) heat 4 and (d) heat 94 and X-direction vibration RMS from 100 to 1000 Hz of (e) heat 4 and of (f) heat 94. These heats were the outliers in Figs. 17 and 18.

temperature and chemical composition of the steel bath was better when compared to using only sub-lance measurements. A support vector machine (SVM)-based black box model was developed in Reference 28 for predicting the bath temperature after the oxygen blow using several input variables and SVM-based multistage modeling was also used in Reference 29 to predict process smelting temperature and five process quality component contents (C, Mn, Si, S, and P) using 22 input features. A data-based predictive model for the BOF

process was also reported in Reference 30. Although the details of the model training in Reference 30 were not revealed, it utilized tens of input variables (including the lance vibration, audio measurements from the top of the lance, and off-gas temperature) and produced as outputs the path temperature (standard dev. 16.2 °C), phosphorus content of the heat (standard dev. 25 ppm), carbon content of the heat (standard dev. 55 ppm), and the iron content of the slag (standard dev. 1.4 pct). In Reference 31, a model was constructed for predicting the needed

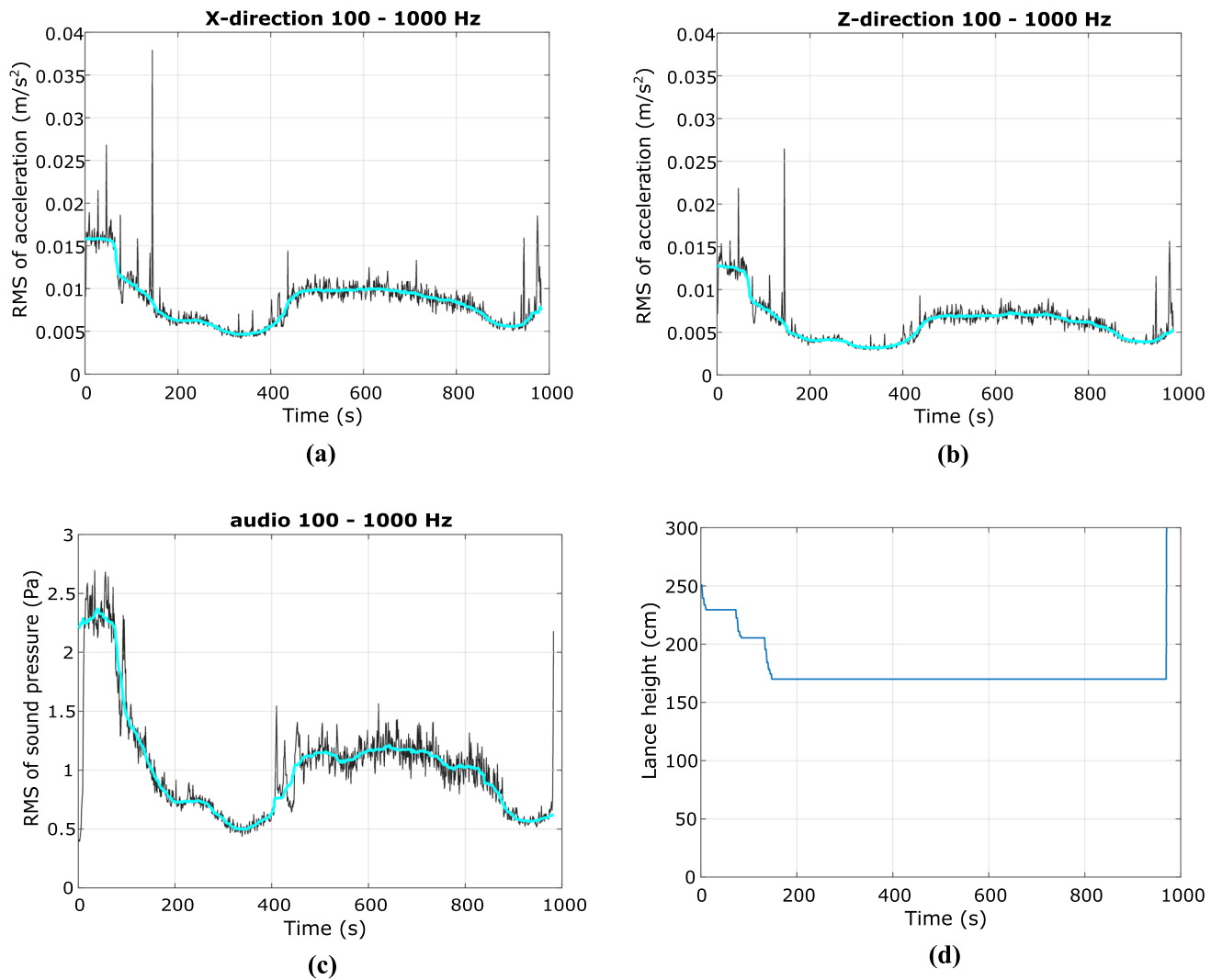


Fig. 21—Heat 182. (a) X-direction vibration RMS from 100 to 1000 Hz, (b) Z-direction vibration RMS from 100 to 1000 Hz, (c) audio RMS from 100 to 1000 Hz, and (d) lance height. This heat was an outlier in Fig. 18.

oxygen volume and coolant addition amount for each heat. In one study^[32] neural networks were used for training a predictive model for the BOF process endpoint bath temperature and carbon content and in Reference 33 generalized linear models with a small number of input and training data were used for the same purpose. Deep neural networks were also utilized in Reference 34 to predict the endpoint bath temperature and carbon content using the continuous spectrum information of the converter mouth flame as an input. A multiple linear regression (MLR) model was developed in Reference 35 to predict phosphorus partitioning in the slag using several input features (temperature, CaO, MgO, SiO₂, Fe, MnO, Al₂O₃, TiO₂, V₂O₅). A mathematical model based on metallurgical reactions was developed in Reference 21 for bath temperature and carbon content prediction utilizing silicon, manganese, oxygen injection rate, and oxygen lance height as extra parameters. Using 37 heats for training and 30 heats for testing, the model reached 82.6 pct accuracy for carbon when endpoint carbon was less than 0.1 wt pct and

85.7 pct when endpoint carbon was between 0.1 and 0.7 wt pct. Several different machine learning algorithms were trained in Reference 36 on a massive dataset of 17000 heats and 33 input parameters of which 5 were time series recorded during the oxygen blow (outdoor temperature, CO and CO₂ levels of the off-gas, lance cooling water temperature, and lance height). The recorded accuracy of their method was 88 pct for target temperature, 92 pct for carbon, and 89 pct for phosphorus.

None of the papers^[21,27–33,35,36] used vibration or sound measurements to support the modeling. Based on the reported good results in References 27, 30, 34, and 36, it is probably very advantageous to include online measurements into the predictive models of the BOF process. One early example of the use of online measurements is Reference 37, where the control of slag formation based on lance vibration previously reported in Reference 5 was combined with sub-lance measurements to fully automate the BOF process. Vibration

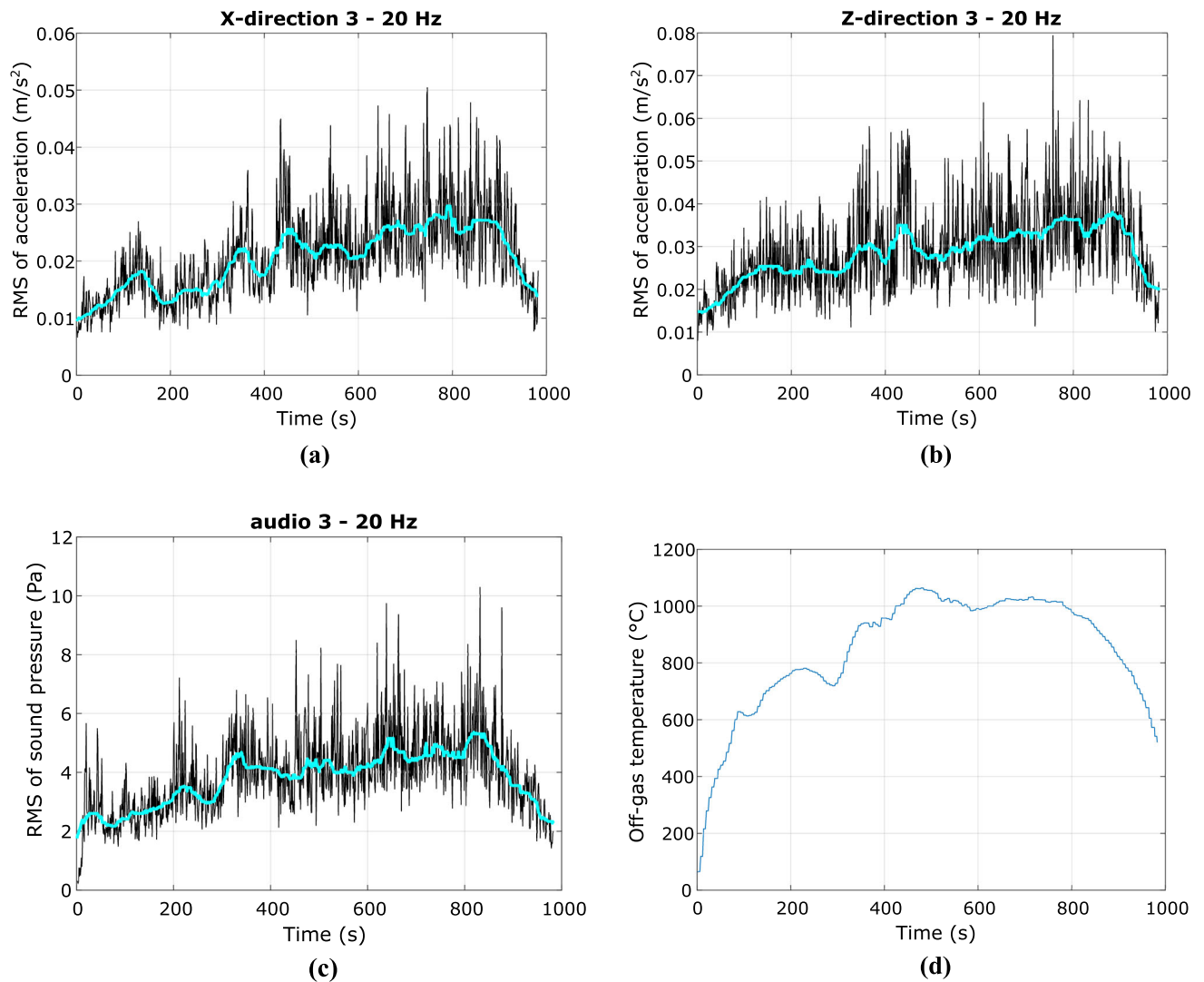


Fig. 22—Heat 182. (a) X-direction vibration RMS from 3 to 20 Hz, (b) Z-direction vibration RMS from 3 to 20 Hz, (c) audio RMS from 3 to 20 Hz, and (d) off-gas temperature.

measurements can also be used to monitor for example the condition of the trunnion ring bearings and the bearings of the tilting drive.^[38]

D. Challenges of Permanent Installation

The two biggest problems with the vibration measurement system were power banks and portable hard drives. These problems are the main reasons for preventing the tested measurement system to be used continuously under steel plant conditions. Even if one could get power banks to operate reliably, they would still need mechanical care every day. Portable hard drives are obviously out of question if vibration measurements are to be used to control the BOF process in real time. Certain problems with the portable hard drives were also noticed during our campaign. For a couple of times a portable hard drive shut itself down and data filled the hard drive of CompactRIO. These problems probably happened because we exceeded the operating temperatures given by the hard drive

manufacturer (5 °C to 35 °C). Changing the power banks and hard drives proved to be cumbersome in the harsh conditions of the steel plant.

Fixed wiring for electricity and data transmission is out of question because of the rotating BOF. This together with the inconvenience of the tested power banks and hard drives suggest that a wireless solution would be more viable. Going wireless would also give the extra benefit of getting part of the equipment farther away from the heat of the BOF. A wireless charger should be placed so that it is charging when the BOF is in the position where it stays most of the time. That would be the upright position, the one where the BOF is during oxygen blowing. Harsh circumstances of a steel plant (dust and heat) need to be taken into consideration. The use of audio measurements is in this regard a lot simpler solution.

Simplest solution for wireless data transmission would be one-way communication where measurement data are transmitted from the vibration sensor to the steel plant control room and processed there. Using specific

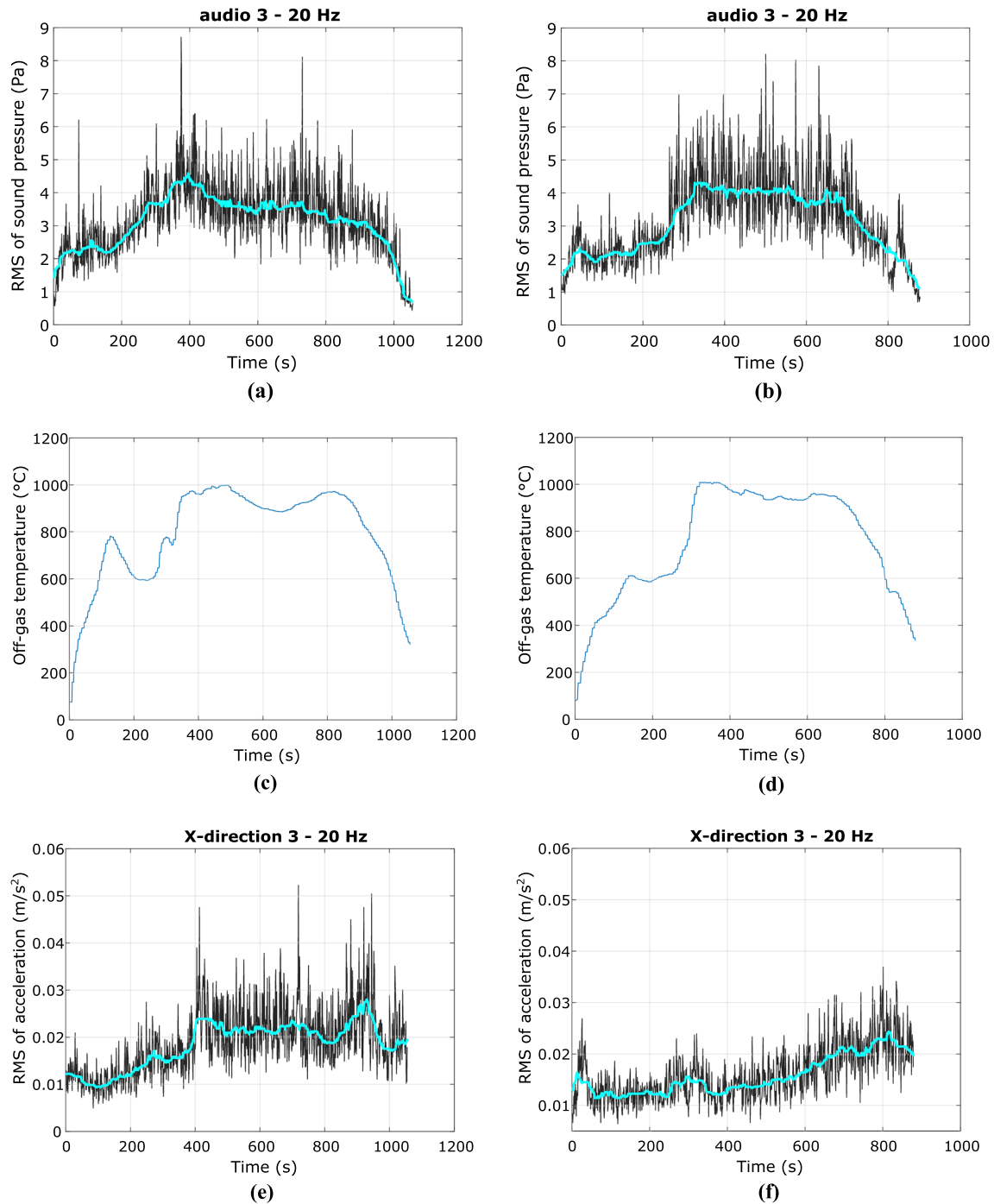


Fig. 23—The audio RMS from 3 to 20 Hz of (a) heat 4 and (b) heat 94, off-gas temperature of (c) heat 4 and (d) heat 94 and X-direction vibration RMS from 3 to 20 Hz of (e) heat 4 and of (f) heat 94.

components instead of CompactRIO could significantly reduce power in-take from the measured 12 watts of our test equipment. These specific components would include a sensor interface providing operating voltage to the sensor and amplifying vibration signals, AD conversion, and coding for radio transmission and finally a radio

transmitter with a corresponding receiver. There are already commercially available wireless battery-powered devices that combine sensors, data collector, and radio into one small unit, though specifications (sensor bandwidth, data storage size, etc.) of those devices are vastly inferior to our test apparatus.

IV. CONCLUSIONS

A measurement system based on sound and mechanical vibration was developed and piloted in an industrial scale BOF. The sound measurements were carried out on top of the vessel by a microphone with a wide linear frequency range, while the vibration measurements were carried out on the undriven side of the vessel at the end of the trunnion pin. The measurement data were stored on a hard drive located in the same housing with the measurement unit. The vibration measurement system was powered by batteries located in a separate housing. Based on a pre-measurement campaign, it was concluded that considerable damping occurs when the vibration signal passes through the trunnion bearing and thus it is indeed favorable to monitor the vibration from the rotating trunnion directly.

Several significant correlations were found between the process variables and vibration and audio measurements. Median filtered low-frequency (3–20 Hz) audio as well as X- and Z-direction acceleration RMS time series correlate with the off-gas temperature, although this is much more significant for the audio data. Median filtered mid-frequency (100–1000 Hz) audio as well as acceleration RMS time series from all directions correlate with the lance height measurement during the interval 20–600 seconds from the beginning of the oxygen blow. For three outlier heats this correlation was not good. These three heats were examined in more detail, and they had increased activity in this frequency range starting about 300 or 400 seconds after the start of the oxygen blow. The audio and vibration activity in this frequency range is possibly related to formation of the metal–slag–gas foam and maybe even to slopping. These results can be refined in further analysis and then be used to augment the existing control system of the BOF process. The foam generation plays an important role for the kinetics of the BOF process and thus a controlled foam generation is a prerequisite for efficient BOF operating practice. Further research can also evaluate the potential for utilizing the suggested vibration and audio features in predicting the endpoint temperature and chemical composition.

The two main problems with the vibration measurement system were power banks and portable hard drives, which, at this point, prevented the measurement to be implemented in continuous operation. More specifically, the power banks require mechanical care on a daily basis to operate reliably, while portable hard drives are ill-suited for online use. From the maintenance point of view, the use of audio measurements turned out to be a much simpler solution than the vibration measurements.

ACKNOWLEDGMENTS

This study was conducted within the framework of the DIMECC Flexible and Adaptive Operations in Metal Production (FLEX) and Towards Fossil-Free Steel (FFS) projects funded by Business Finland.

SSAB Europe Oy is gratefully acknowledged for supporting this work.

FUNDING

Open Access funding provided by University of Oulu including Oulu University Hospital.

CONFLICT OF INTEREST

The authors declare that they have no conflict of interest.

OPEN ACCESS

This article is licensed under a Creative Commons Attribution 4.0 International License, which permits use, sharing, adaptation, distribution and reproduction in any medium or format, as long as you give appropriate credit to the original author(s) and the source, provide a link to the Creative Commons licence, and indicate if changes were made. The images or other third party material in this article are included in the article's Creative Commons licence, unless indicated otherwise in a credit line to the material. If material is not included in the article's Creative Commons licence and your intended use is not permitted by statutory regulation or exceeds the permitted use, you will need to obtain permission directly from the copyright holder. To view a copy of this licence, visit <http://creativecommons.org/licenses/by/4.0/>.

REFERENCES

1. T.W. Miller, J. Jimenez, A. Sharan, and D.A. Goldstein: in *The Making, Shaping and Treating of Steel, Steelmaking and Refining Volume, Chapter 9 Oxygen Steelmaking Processes*, R.J. Fruehan, ed., 11th ed., The AISE Steel Foundation, Pittsburgh, PA, 1998, pp. 475–524. https://www.academia.edu/37434608/Steelmaking_and_Refining_Volume_AISE_1998.
2. G. Snigdha, B.N. Bharath, and N.N. Viswanathan: *Miner. Process. Extr. Metall.*, 2019, vol. 128(1–2), pp. 17–33. <https://doi.org/10.1080/25726641.2018.1544331>.
3. H. Jalkanen and L. Holappa: *Converter steelmaking, Treatise on process metallurgy, vol. 3: Industrial Processes*, Chapter 1.4, Elsevier, 2014, pp. 223–70. <https://doi.org/10.1016/B978-0-08-096988-6.00014-6>.
4. S.C. Koria and K.W. Lange: *Steel Res.*, 1987, vol. 58(9), pp. 421–26.
5. Y. Iida, K. Emoto, M. Onishi, K. Hirayama, M. Okawa, and H. Yamada: *Trans. Iron Steel Inst. Jpn.*, 1980, vol. 20, p. 31.
6. M. Brämning, S. Millman, A. Overbosch, A. Kapilashrami, D. Malmberg, and B. Björkman: *ISIJ Int.*, 2011, vol. 51(1), pp. 71–79. <https://doi.org/10.2355/isijinternational.51.71>.
7. M. Brämning, G. Parker, S. Millman, A. Kapilashrami, D. Malmberg, and B. Björkman: *Steel Res Int.*, 2011, vol. 82(6), pp. 683–92. <https://doi.org/10.1002/srin.201000275>.
8. S. Sabah and G. Brooks: *Ironmak. Steelmak.*, 2016, vol. 43(6), pp. 473–80. <https://doi.org/10.1080/03019233.2015.1113755>.
9. L. De Vos, V. Cnockaert, I. Bellemans, C. Vercruyssen, and K. Verbeken: *Steel Res. Int.*, 2021, vol. 92(1), p. 2000282. <https://doi.org/10.1002/srin.202000282>.

10. W. Birk, I. Arvanitidis, P.G. Jönsson, and A. Medvedev: *IEEE Trans Ind. Appl.*, 2001, vol. 37(4), pp. 1067–73. <https://doi.org/10.1109/28.936398>.
11. P.E. Nilles and P.H. Dauby: *Iron Steel Eng.*, 1976, vol. 3, pp. 42–47.
12. J. Claes and P. Dauby: *Proceedings of the McMaster symposium on Iron and Steelmaking No. 9 Symposium on BOF end point determination*, McMaster University Press, Hamilton, ON, 20–21 May 1981.
13. A.G. Velichko, V.I. Baptizmanskii, V.D. Antonets, and A. Markotic: *Metalurgija*, 1997, vol. 36(2), pp. 77–82.
14. F. Mucciardi and G. Barrera: *Proceedings of the 67th Steelmaking Conf.*, Iron and Steel Society, Chicago, IL, 1984, vol. 67, pp. 221–29.
15. F. Mucciardi, V. Krujelskis, and E. Palumbo: *Proceedings of the 5th 'Process Technol.' Conf.*, ISS/AIME, Detroit, MI, 1985, pp. 85–90.
16. K. O'Leary and F. Mucciardi: *Proceedings of the 6th 'Process Technol.' Confer.*, ISS/AIME, Washington, DC, 1986, pp. 285–92.
17. J. Heenatimulla, G.A. Brooks, M. Dunn, D. Sly, R. Snashall, and W. Leung: *Metals*, 2022, vol. 12(7), p. 1142. <https://doi.org/10.3390/met12071142>.
18. S. Miller and D. Childers: *Probability and Random Processes: With Applications to Signal Processing and Communications*, 2nd ed. Academic Press, Burlington, 2012, pp. 473–516.
19. B. Sarma, R. C. Novak, and C. L. Bermel: *Proceedings of the 79th Steelmaking Conference*, Iron and Steel Society, Pittsburgh, PA, 1996, pp. 115–22.
20. D. Daring, C. Swartz, and N. Dogan: *Processes*, 2020, vol. 8(4), p. 483. <https://doi.org/10.3390/pr8040483>.
21. G.-H. Li, B. Wang, Q. Liu, X.-Z. Tian, R. Zhu, N. Li, and G.-G. Cheng.: *Int. J. Miner. Metall. Mater.*, 2010, vol. 17(6), pp. 715–22. <https://doi.org/10.1007/s12613-010-0379-4>.
22. N. Molloy: *J. Iron Steel Inst.*, 1970, vol. 208(10), pp. 943–50.
23. D.E. Hinkle, W. Wiersma, and S.G. Jurs: *Applied Statistics for the Behavioral Sciences*, 5th ed. Houghton Mifflin, Boston, 2003.
24. B. Efron: *Ann. Stat.*, 1979, vol. 7, pp. 1–26. <https://doi.org/10.1214/aos/1176344552>.
25. K. Koch, W. Fix, and P. Valentin: *Stahl Eisen*, 1976, vol. 47(11), pp. 659–63.
26. N. Dogan: *Mathematical Modelling of Oxygen Steelmaking*, Doctoral thesis, Swinburne University of Technology, Melbourne, 2011.
27. I. Tanaka, Y. Jono, M. Kanemoto, and T. Yoshida: *Proceedings of the McMaster symposium on Iron and Steelmaking No. 9 Symposium on BOF end point determination*, McMaster University Press, Hamilton, ON, 20–21 May 1981.
28. J. Valyon and G. Horváth: *IEEE Trans Instrum. Meas.*, 2009, vol. 58(8), pp. 2611–17.
29. C. Liu, L. Tang, J. Liu, and Z. Tang: *IEEE Trans Autom. Sci. Eng.*, 2019, vol. 16(3), pp. 1097–1109.
30. H.-J. Odenthal, N. Uebber, J. Schlüter, M. Löpke, K. Morik, and H. Blom: *Stahl Eisen*, 2014, vol. 134(8), pp. 62–67.
31. M. Han, Y. Li, and Z. Cao: *Neurocomputing*, 2014, vol. 123, pp. 415–23.
32. X. Ding, J. Wang, and S. Yang: *Proceedings of the 2nd International Symposium on Knowledge Acquisition and Modeling*, IEEE Computer Society, Wuhan, 2009.
33. S. Xie and T. Chai: *Proceedings of the 14th Triennial IFAC World Congress*, IFAC Proceedings Volumes, vol. 32 (2), Beijing, 5–9 July 1999, pp. 7039–43.
34. Y. Han, C.-J. Zhang, L. Wang, and Y.-C. Zhang: *IEEE Trans Industr. Inform.*, 2020, vol. 16(4), pp. 2640–50.
35. S. Barui, S. Mukherjee, and K. Chattopadhyay: *Proceedings of the 8th International Conference on Modeling and Simulation of Metallurgical Processes in Steelmaking (STEELSIM 2019)*, Association for Iron and Steel Technology (AIST), Toronto, ON, 13–15 August 2019.
36. J. Bae, Y. Li, N. Ståhl, G. Mathiason, and N. Kojola: *Metall. Mater. Trans. B*, 2020, vol. 51B, pp. 1632–45. <https://doi.org/10.1007/s11663-020-01853-5>.
37. Y. Iida, K. Emoto, M. Okawa, Y. Masuda, M. Onishi, and H. Yamada: *Trans Iron Steel Inst. Jpn.*, 1984, vol. 24(7), pp. 540–46. <https://doi.org/10.2355/isijinternational1966.24.540>.
38. F. Hartl, A. Mayrhofer, A. Rohrhofer, and K. Stohl: *Proceedings of the 3rd ESTAD Conf.*, Austrian Society for Metallurgy and Materials (ASMET), Vienna, 26–29 June 2017.

Publisher's Note Springer Nature remains neutral with regard to jurisdictional claims in published maps and institutional affiliations.